

Subscriber access provided by Helmholtz Zentrum Muenchen - Zentralbibliothek

Article

Integrative proteomics and targeted transcriptomics analyses in cardiac endothelial cells unravel mechanisms of long-term radiation-induced vascular dysfunction

Omid Azimzadeh, Wolfgang Sievert, Hakan Sarioglu, Juliane Merl-Pham, Ramesh Yentrapalli, Mayur V. Bakshi, Dirk Janik, Marius Ueffing, Michael J. Atkinson, Gabriele Multhoff, and Soile Tapio

J. Proteome Res., Just Accepted Manuscript • DOI: 10.1021/pr501141b • Publication Date (Web): 15 Jan 2015

Downloaded from http://pubs.acs.org on January 27, 2015

Just Accepted

"Just Accepted" manuscripts have been peer-reviewed and accepted for publication. They are posted online prior to technical editing, formatting for publication and author proofing. The American Chemical Society provides "Just Accepted" as a free service to the research community to expedite the dissemination of scientific material as soon as possible after acceptance. "Just Accepted" manuscripts appear in full in PDF format accompanied by an HTML abstract. "Just Accepted" manuscripts have been fully peer reviewed, but should not be considered the official version of record. They are accessible to all readers and citable by the Digital Object Identifier (DOI®). "Just Accepted" is an optional service offered to authors. Therefore, the "Just Accepted" Web site may not include all articles that will be published in the journal. After a manuscript is technically edited and formatted, it will be removed from the "Just Accepted" Web site and published as an ASAP article. Note that technical editing may introduce minor changes to the manuscript text and/or graphics which could affect content, and all legal disclaimers and ethical guidelines that apply to the journal pertain. ACS cannot be held responsible for errors or consequences arising from the use of information contained in these "Just Accepted" manuscripts.



Integrative proteomics and targeted transcriptomics analyses in cardiac endothelial cells unravel mechanisms of long-term radiation-induced vascular dysfunction

Omid Azimzadeh¹, Wolfgang Sievert², Hakan Sarioglu³, Juliane Merl-Pham³, Ramesh Yentrapalli¹, Mayur V. Bakshi¹, Dirk Janik⁴, Marius Ueffing^{3,5}, Michael J. Atkinson^{1,6}, Gabriele Multhoff², and Soile Tapio¹

¹Helmholtz Zentrum München - German Research Centre for Environmental Health, Institute of Radiation Biology, Neuherberg, Germany

²Department of Radiation Oncology, Klinikum rechts der Isar, Technische Universität München, Munich, Germany and Clinical Cooperation Group (CCG) "Innate Immunity in Tumor Biology", Helmholtz Zentrum München, Deutsches Forschungszentrum für Gesundheit und Umwelt, Munich, Germany

³Helmholtz Zentrum München - German Research Centre for Environmental Health, Research Unit Protein Science, Neuherberg, Germany

⁴Helmholtz Zentrum München, German Research Centre for Environmental Health, Institute of Pathology, Neuherberg, Germany

⁵Centre of Ophthalmology, University Medical Centre, Tuebingen, Germany

⁶Chair of Radiation Biology, Technical University of Munich, Munich, Germany

To whom correspondence should be addressed:

E-mail: omid.azimzadeh@helmholtz-muenchen.de

Phone: +49-89-3187-3887; Fax: +49-89-3187-3378

Key words: ionising radiation, proteomics, ICPL, insulin, PI3K, PPAR alpha, endothelial cell, endothelial cell dysfunction, heart, cardiovascular disease

Abbreviations: CVD, cardiovascular disease; EC, endothelial cell; GO, Gene Ontology; Gy, gray; ICPL, isotope-coded protein label; LC-ESI-MS/MS, liquid chromatography-electron spray ionisation-mass spectrometry; NO, nitric oxide

Abstract

Epidemiological data from radiotherapy patients show the damaging effect of ionising radiation on heart and vasculature. The endothelium is the main target of radiation damage and contributes essentially to the development of cardiac injury. However, the molecular mechanisms behind the radiation-induced endothelial dysfunction are not fully understood. In the present study, 10-week old C57Bl/6 mice received local X-ray heart doses of 8 or 16 Gy and were sacrificed after 16 weeks; the controls were sham-irradiated. The cardiac microvascular endothelial cells were isolated from the heart tissue using streptavidin-CD31 coated micro-beads. The cells were lysed and proteins were labelled with duplex isotope coded protein label methodology for quantification. All samples were analysed by LC-ESI-MS/MS and Proteome Discoverer software. The proteomics data were further studied by bioinformatics tools and validated by targeted transcriptomics, immunoblotting, immunohistochemistry, and serum profiling. Radiation-induced endothelial dysfunction was characterised by impaired energy metabolism and perturbation of the insulin/IGF-PI3K-Akt signalling pathway. The data also strongly suggested premature endothelial senescence, increased oxidative stress, decreased NO availability and enhanced inflammation as main causes of radiation-induced long-term vascular dysfunction. Detailed data on molecular mechanisms of radiation-induced vascular injury as compiled here are essential in developing radiotherapy strategies that minimise cardiovascular complications.

Introduction

Epidemiological studies indicate that high and moderate local doses (>0.5 Gy) of ionising radiation to the heart increase the risk of cardiovascular disease (CVD). Adverse effects are observed in patients after thoracic radiotherapy for breast cancer, Hodgkin's disease or a number of childhood cancers. ¹⁻⁴ Due to novel post-operative methods, ⁵ the heart dose from left-tangential radiotherapy has been reduced. However, certain parts of the heart still receive more than 20 Gy if the cancer is localised on the left thoracic side of the patient. ⁶ Since breast cancer is one of the most common tumours and the age of this patient group is relatively low, there is a high estimated risk of developing radiation-induced CVD later in life. ⁵ Therefore, a deeper insight of the molecular mechanisms of CVD following irradiation of the heart is urgently needed.

Human and animal data indicate the important role of vascular injury and endothelial dysfunction in the pathogenesis of radiation-induced CVD. ⁷⁻¹² Endothelial dysfunction refers to a complex pathological condition that is characterised by series of events including endothelial barrier impairment, impaired vasodilation and vasoconstriction, reduced nitric oxide (NO) production, increased expression of adhesion molecules, elevated level of cytokines, and increased reactive oxygen species production from the endothelium. ^{13, 14} Insulin signal transduction pathway in vascular endothelium regulates the endothelial NO production via PI3K-Akt cascade. ^{15, 16} It is also an upstream regulator of MAP kinase signalling that is involved in the endothelial vasoconstriction, adhesion and inflammation. ¹⁷ Homeostasis between insulin-dependent PI3K signalling and insulin-dependent MAP kinase signalling pathways governs the main endothelial functions: vasodilation and vasoconstriction. ¹⁸

Endothelial dysfunction contributes to pro-fibrotic and pro-inflammatory environments that are common features of radiation-induced tissue injury. ^{19, 20} Oxidative stress, increased levels of endothelial adhesion molecules, inflammation and cellular senescence are all

consequences of normal aging ²¹ that occur much earlier in irradiated tissues ²² including the heart. ²³ These data indicate an intensification and acceleration of age-related molecular processes.

There is accruing evidence indicating the role of endothelial dysfunction in both macro- and microvascular damage after irradiation. ^{12, 24} It has been demonstrated that high-dose radiation results in endothelial cell loss and decrease in microvascular density in murine heart. ²⁵ We have previously shown using an *in vitro* cellular system that irradiation alters stress-induced signalling pathways including Rho GTPase ²⁶⁻²⁸ and MAP kinase ^{10, 29} pathways in endothelial cells (EC). Furthermore, chronic low-dose-rate ionising radiation accelerated the premature endothelial senescence *in vitro*, associated with the deactivation of the PI3K-Akt signalling cascade. ^{29, 30}

However, endothelial cell lines and primary endothelial cells proliferate rapidly *in vitro* ^{22, 31} and thus may not reflect the response of slowly proliferating endothelial cells of adult organs on ionising irradiation.

To address this issue we here investigated molecular mechanisms leading to radiation-induced endothelial dysfunction using an *ex vivo* experimental design where the analysis was made using ECs directly isolated from the heart. For this purpose, C57BL/6 mice were exposed to local heart irradiation at clinically relevant X-ray doses of 8 and 16 Gy, whereas control mice were sham irradiated. To avoid of losing animals ¹²,primary microvascular endothelial cells were isolated from irradiated and non-irradiated hearts ³¹ 16 weeks after the exposure. The investigation of the purified primary endothelial cells included quantitative proteomics analysis that was further completed by targeted transcriptomics and verified by immunoblotting, bioinformatics, immunohistochemistry and serum profiling.

Our data indicate that radiation-induced endothelial dysfunction is associated with deactivation of insulin-dependent PI3K signalling and insulin-dependent MAP kinase signalling pathways. We further show that endothelial injury caused by ionising radiation is

characterised by increased senescence, enhanced oxidative stress, inflammation and impaired NO signalling. Our results emphasise the role of early vascular dysfunction in the heart pathology after radiation exposure.

Experimental section

Materials

Beta-octylglucoside, SDS, and ammonium bicarbonate were obtained from Sigma (St. Louis, MO); RapiGest from Waters (USA); acetone, acetonitrile, formic acid, and trifluoroacetic acid (TFA) from Roth (Karlsuhe, Germany); dithiothreitol (DTT), iodoacetamide, tris-(hydroxymethyl) aminomethane (Tris) and sequencing grade trypsin were obtained from Promega (Madison, WI); cyano-4-hydroxycinnamic acid was obtained from Bruker Daltonik (Bremen, Germany). All solutions were prepared using HPLC grade water from Roth (Karlsuhe, Germany).

Animals

All experiments were approved by the "Regierung von Oberbayern" (Certificate No. 211-2531-54/01) and were performed in accordance with institutional guidelines of the Klinikum rechts der Isar, Technische Universität München. 10-week-old male C57Bl/6 mice (Charles River) received local cardiac irradiation with a single X-ray dose of 8 or 16 Gy (200 kV, 10 mA); age-matched control mice received sham irradiation. Each mouse was immobilised without anaesthetic in a specially designed jig. Preceding the exposure the position of the heart inside the jig was localised by digital radiographs. The heart irradiation field consisted of a 9 x 13 mm² window in a lead plate of 2 mm of thickness. The animals were sacrificed by cervical dislocation 16 weeks after irradiation. In total, 90 animals with 30 animals in each group were used in this study.

Isolation of cardiac microvascular endothelial cells and serum

The heart was rinsed with phosphate buffered saline, and the cardiac microvascular endothelial cells (ECs) were isolated as described before. ³¹ Briefly, viable primary ECs were isolated using streptavidin-CD31-coated microbeads after mechanic and enzymatic digestion of the heart tissue and tested for purity by fluorescence-activated cell sorting (FACS) analysis. For all proteomics and gene analyses, harvested cells from 3 animals belonging to the same group (controls, 8 Gy- and 16 Gy-irradiated samples) were pooled separately into one batch. Each pooled batch was used as a single biological replicate. Freshly isolated primary microvascular ECs were phenotypically characterised by flow cytometry using a FACSCalibur instrument (BD, Heidelberg, Germany) with the following fluorescein (FITC), phycoerythrin (PE) or allophycocyanin (APC) conjugated antibodies: CD31 (PECAM-1, BD Bioscience, clone MEC 13.3), CD34 (mucosialin, eBioscience, clone RAM34), CD54 (ICAM-1, BD Bioscience, clone 3E2), CD102 (ICAM-2, BD Bioscience, clone 3C4), CD105 (endoglin, eBioscience, clone MJ7/18), CD106 (VCAM-1, Life Technologies, clone M/K-2) and CD144 (VE-cadherin, BD Bioscience, clone 11D4.1). Further, CD45 (leukocyte common antigen, BD Bioscience, clone 30-F11) was used to prove purity. Appropriately labelled isotype-matched immunoglobulins were used as negative controls. Briefly, 0.1 x 10⁶ viable cells were incubated with the indicated antibodies for 30 min at 4°C in the dark. Following a washing step in PBS/FCS (10%) cells were analysed with a FACSCalibur instrument. Dead cells were excluded from the analysis by a propidium iodide co-staining and gating strategy.

After sacrificing the mice by cervical dislocation, blood was rapidly removed by cardiocentesis. For serum isolation the blood was centrifuged at 2000 rpm for 10 min after clotting and stored at -80°C for further analysis. For all analyses three serum samples were pooled and used as a single biological replicate.

Proteomics

Protein Extraction

Proteins were isolated with ICPL lysis buffer following the manufacturer's instructions (SERVA). Protein concentration was determined by Bradford assay following the manufacturer's instructions (Thermo Fisher).

Protein ICPL labelling and resolution

The labelling was done as previously reported. ³² Briefly, triplicate aliquots of 50 µg of cell lysate proteins obtained from either control or irradiated mice were labelled with ICPL reagents (SERVA) following the manufacturer's instructions. ICPL0 was used for control samples and ICPL6 for irradiated samples according to the manufacturer's protocol. To evaluate the biological and technical reproducibility of proteomics analysis, a protein mixture with known ratios of heavy and light label containing bovine serum albumin (1:1), chicken ovalbumin (4:1) and bovine carbonic anhydrase II (1:2) was used as an internal standard prior labelling. The labelling was done using three biological replicates.

The heavy and light labelled samples were combined, and separated by 12% SDS gel electrophoresis before staining with colloidal Coomassie solution. SDS-PAGE lanes were cut into 5 slices. Prior to digestion, proteins were de-stained and digested overnight with trypsin as described before. ³³ Peptides were extracted and acidified for subsequent mass spectrometry analysis.

LC-ESI-MS/MS analysis

The digested peptides were separated by reversed phase chromatography (PepMap, 15 cm x 75 μ m ID, 3 μ m/100Å pore size, LC Packings) operated on a nano-HPLC (Ultimate 3000, Dionex) with a nonlinear 170 min acetonitrile (ACN) gradient in 0.1% formic acid (FA) in water at a flow rate of 300 nl/min. The gradient settings were subsequently: 0-140 min: 5-31 % ACN, 140-150 min: 31-93% ACN, followed by equilibration for 20 min at starting conditions. The nano-LC was connected to a linear quadrupole ion trap-Orbitrap (LTQ Orbitrap XL) mass spectrometer (Thermo Fisher, Bremen, Germany) equipped with a nano-ESI source.

The mass spectrometer was operated in the data-dependent mode to automatically switch between Orbitrap-MS and LTQ-MS/MS acquisition. The following mass spectrometer settings were used: Mass window: 300 – 1500 m/z, charge state settings: Default charge state +2; rejection of unassigned charge states and +1; all +2 and more allowed normalized collision energy: 35. Survey full scan MS spectra (from m/z 300 to 1500) were acquired in the Orbitrap with resolution R = 60,000 at m/z 400. The method used allowed sequential isolation of the most intense ions, up to ten, depending on signal intensity, for fragmentation on the linear ion trap using collision-induced dissociation. High resolution MS scans in the Orbitrap and MS/MS scans in the linear ion trap were performed in parallel. Target peptides already selected for MS/MS were dynamically excluded for 60 seconds.

The acquired MS/MS spectra were searched against the Ensembl *Mus musculus* database using an in-house version of Mascot (Matrix Science, version 2.3.02; 20121023, Number of residues: 26203053; Number of sequences: 56416) with the following parameters: MS/MS spectra were searched with a precursor mass tolerance of 10 ppm and a fragment tolerance of 0.8 Da; Arg-C was selected as enzyme. One missed cleavage was allowed and carbamidomethylation was set as a fixed modification. Oxidised methionine and the heavy and light ICPL labels of lysines as well as heavy and light labels of the protein N-terminus were set as variable modifications.

Quantification with ICPL

Data processing for protein identification and quantification of ICPL pairs was performed using Proteome Discoverer version 1.3 (Thermo Fisher) as described before. ³² Briefly, the software provides automated strict statistical analysis of the protein quantification using only unique peptides. To minimise experimental bias the software was set to normalise on the protein median (minimum protein count: 20). The complete peptide and protein profiles were filtered using high peptide confidence and top one peptide rank filters. The false discovery rate (FDR) was calculated at the peptide level for all experimental runs using the Decoy option in Mascot; this rate was estimated to be lower than 1% using the identity threshold as

the scoring threshold system. The MASCOT Percolator algorithm was used for discriminating between correct and incorrect spectrum identifications ³⁴ with a maximum *q* value of 0.01. Due to these criteria, the ICPL method noticeably lowered the significance level of a protein score and increased the probability of a significant protein hit. Differentially-labelled isotopic pairs were detected with a mass precision of 2 ppm and a retention time window of 0.3 min. The calculated peptide ratio variability in the Proteome Discoverer software is an alternative of coefficient of variation (CV) used to calculate a particular protein ratio. For the quantification data as replicates, software calculates the protein ratios for single searches as CV for log-normal distributed data and then calculates the classical coefficient variation for these ratios. The average heavy/light ratio and ratio variability were applied for protein quantification wherever multiple peptides were identified for a protein. The proteins identified by at least 2 unique "high confidence" identified peptides in two out of three replicates were considered for further evaluation.

The H/L ratios associated with significant variation of protein expression were determined as described before. ^{10, 35} Briefly, the significant fold changes were determined by technical variability based on the average values of the CV of spiked standard protein mixture. The CV% obtained for H/L ratios of spiked proteins were 18.6% (8 Gy), and 15.2% (16 Gy). We considered the variability of 30-40% (>2 CV) as significant as it overcame technical variability in our experiments. Accordingly, proteins with H/L ratios greater than 1.3-fold or less than 0.7-fold were defined as significantly differentially expressed.

Protein-protein interaction and signalling network

The analyses of protein-protein interaction and signalling networks were performed by the software tool INGENUITY Pathway Analysis (IPA) (INGENUITY System, http://www.INGENUITY.com). IPA is a knowledge database generated from peer-reviewed scientific publications that enables discovery of highly represented functions and pathways (p < 0.001) from large quantitative data sets. ³⁶ The analysis of protein–protein interaction

and signalling networks was performed by the search tool STRING version 9.1 (http://string-ub.org) coupled to the Reactome database (http://www.reactome.org). ³⁷

Pathway-focussed gene expression profiling with qRT-PCR

Total RNA was extracted from control and the 8 Gy- and 16 Gy- irradiated cardiac vascular endothelial cells using the mirVana[™] miRNA isolation kit (Applied Biosystems; Foster City, CA, USA) following the protocol for total RNA isolation. The quantity and quality of the total RNA and miRNA was measured with the Nanodrop spectrophotometer (PegLab Biotechnology; Germany). The mouse senescence and PI3K signaling pathway RT² Profiler PCR arrays (Qiagen) were used to profile the expression of 84 genes related to signalling pathways. Single-stranded cDNA was synthesised from 100 ng of total RNA using the SuperArray reaction ready first strand cDNA synthesis kit. The cDNAs were mixed with SuperArray RT² Real time SYBR Green/ROX PCR master mix and real time PCR performed in accordance with the manufacturer's instructions. Thermal cycling and fluorescence detection were performed using a StepOne Sequence Detection System (Applied Biosystems, Foster City, CA), according to the manufacturer's instructions., and expression of the regulated transcripts were compared between the groups using student's t test. The false discovery rate (FDR) calculation was used to adjust p-values. 38 The calculation was performed using modified BenjaminiHochberg.xlsx created by Manuel Weinkauf (https://marum.de/Software and Programs.html) licensed under a Creative Commons Attribution-NonCommercial-ShareAlike 3.0 Unported License (http://creativecommons.org/licenses/by-nc-sa/3.0/deed.en GB). All p-values below the corrected significance level q^* considered as significant results.

Immunoblotting analysis

Proteins separated by 4-12% SDS-PAGE were transferred to nitrocellulose membranes (GE Healthcare) using a TE 77 semidry blotting system (GE Healthcare) at 1 mA/cm for 1h. The membranes were blocked using 3% BSA in PBS, pH 7.4, for 1 h at room temperature,

washed three times in 10 mM Tris-HCl, pH 7.4, 150 mM NaCl for 5 min and incubated overnight at 4°C with primary antibodies using dilutions recommended by the manufacturer. Immunoblot analysis of EC protein lysate was performed using anti-INSR / IGF1R (ab172965), anti-phospho INSR / IGF1R (Tyr1146/1131) (#3021), anti-PI3K (p85) and antiphospho PI3K [p85 (Tyr458)/p55 (Tyr199)] (#9655), anti-Akt (#9272), anti-phospho AKt (Ser473) (#9271), anti-mTOR, anti-phospho mTOR (Ser2488), anti-GSK3 beta (cs-9315), anti-phospho GSK3 beta (Ser21/9) (cs-9331), anti-FOXO3a (cs-9467), anti-phospho FOXO3a (Ser318/321) (cs-9464), anti-eNOS (#9572), anti-phospho eNOS (Ser1177) (#9571), anti-Glut4 (sc-53566), anti-ERK 44/42(#9102), anti-phospho-ERK (p-ERK) (#9101), anti-p38 (#9212), anti-phospho-p38 (p-p38) (#9211), anti-superoxide dismutase 1 (SOD) (sc11407), anti-heat shock proteins 90 (Hsp90) (#4875), anti-heat shock proteins 70 (Hsp70)(MA3-007), anti-p16 (#4824), anti-p21(#2947) and anti-p53 and anti-phospho-p53 (#9919) and anti-GAPDH (sc-47724). After washing three times, the blots were incubated with either horseradish peroxidase-conjugated or alkaline phosphatase-conjugated antimouse, anti-rabbit or anti-goat secondary antibody (Santa Cruz Biotechnology) for 2 hours at room temperature and developed using the ECL system (GE Healthcare) or 1-step[™] NBT/BCIP method (ThermoFisher) following standard procedures. GAPDH was unchanged in proteomics profiles after 8 Gy and 16 Gy and was therefore used as a loading control. Quantification of digitised images of immunoblot bands from three biological replicates was done using ImageJ (http://rsbweb.nih.gov/ij/).

IRS-1 Phosphorylation status assay

The alteration in the phosphorylation status of insulin receptor substrate 1 (IRS-1) was assessed using PathScan® Phospho-IRS-1 (serine-621, serine-307) and phospho-IRS-1 (pan-tyrosine) Sandwich ELISA Kits. The data were compared to the level of total IRS-1 detected by PathScan® Total IRS-1 Sandwich ELISA Kit (Cell Signaling).

Lipid peroxidation and protein nitrosylation and protein homocysteinylation and protein carbonylation assay

Oxidative stress-induced protein modifications including the malondialdehyde (MDA) formation, protein carbonyl group and 3-nitrotyrosine assay were performed using the assay kits (Biovision) according to the manufacturer's instructions. The level of homocysteinylated endothelial proteins was detected by immunoblotting. Lysates from control and irradiated endothelial cells were loaded on the same gel in similar amounts using same transfer conditions. The amount of the total protein was confirmed by Ponceau S staining for accurate comparison between the three groups. Total intensity of protein bands was quantified using ImageJ software (http://rsbweb.nih.gov/ij/) by integration of all the pixel values in the band area after background correction.

Serum glucose, nitric oxide, cytokines and oxLDL assay

The serum glucose was measured using Cayman glucose colorimetric assay kit (Cayman chemical). For the quantitative determination of bioavailability of the nitric oxide in serum, the total nitrate/nitrite was measured by an *in vitro* enzymatic colorimetric assay (BioVision). The quantitative profiling of the oxidative stress-induced cytokines was performed by an *in vitro* ELISA assay (Signosis). The assay compared the protein expression level of TNF alpha, TGF beta, MCP1, IL1 alpha, IL 1beta, and IL6. The level of oxidised low-density lipoprotein (oxLDL) was measured in serum using oxLDL ELISA kit (My Biosource) following the manufacturer's instructions.

Histology and immunohistochemistry

Myocardial microvessel density (MVD) was measured by immunohistochemical staining for CD31. Three randomised areas of the left ventricular myocardium (0.025 mm²) were chosen for quantification using the criteria of Weidner et al. ³⁹ Any brown-staining of endothelial cells or cell clusters, clearly separate from adjacent microvessels or other tissue elements, was

considered as a single, countable microvessel. The number of vessels counted in any of the areas was recorded and the mean and standard deviation were calculated.

Inflammatory endothelial activation was measured by immunohistochemical staining of the adhesion molecule E-selectin. The expression of E-selectin was graded by evaluating the incidence and intensity of positively stained endothelium of myocardial vessels using the criteria of Tsokos. ⁴⁰ The intensity of the immunostaining was graded as absent (0), weak (1), moderate (2) and strong (3) and the percentage of blood vessels involved per visual field was graded as absent (0), < 10% (1), 10–50% (2) and > 50% (3). The total score was achieved by adding both variables. Each immunohistochemical staining was performed simultaneously with identical incubation times and concentrations for the primary and secondary antibody and diaminobenzidine (DAB) solution.

Statistical analysis

Comparative analysis of the data was carried out using the Student's t-test (two-paired and unpaired). The significance levels were $p^* < 0.05$ (5%); $p^{**} < 0.01$ (1%); $p^{***} < 0.001$ (0.1%). The error bars were calculated as standard error of the mean (SEM). All experiments were done with at least three biological replicates.

Data availability

Access to raw MS data is provided in RBstore (http://www.rbstore.eu), ¹⁰ the radiobiology database, where all MS/MS raw files for this publication are located.

Results

The yield and cell surface marker expression of EC were altered after local heart irradiation

Compared to the age-matched control animals, a significant decrease (15%) in the number of isolated cardiac microvascular ECs was observed in the group of mice that were irradiated

with 16 Gy but not at 8 Gy (Figure 1). Primary ECs from all groups were characterised directly after isolation by flow cytometric analysis using EC-specific antibodies directed against PECAM-1, endoglin, VE-cadherin, ICAM-1, ICAM-2, mucosialin and VCAM-1. The leukocyte marker was not detectable in any population of isolated ECs (data not shown). The proportion of cells that stained positively for PECAM-1, endoglin, VE-cadherin, ICAM-1, ICAM-2 and mucosialin was nearly 100% (97±2), independent of the radiation dose (Figure 2 A). The proportion of ECs that stained positively for VCAM-1 was only around 40% in all groups and modestly but significantly increased after 8 Gy (32%) compared with control ECs. Analysis of the cell surface densities of both intercellular adhesion molecues ICAM-1 and ICAM-2 showed significant increases after 16 weeks at 8 Gy (44 and 71%, respectively) and 16 Gy (55 and 69%, respectively) compared to control ECs (Figure 2 B).

The irradiation altered endothelial proteome

The ICPL method was used to investigate radiation-induced changes in the cardiac endothelial proteome. The proteins with H/L ratios greater than 1.3-fold or less than 0.7-fold were defined as significantly differentially expressed. ^{10, 35} The heavy / light (H/L) ratio and coefficient of variation (CV%) of spiked proteins in different replicates and the complete lists of significantly deregulated proteins and all identified and quantified peptides are shown in the Tables S1- S5.

After local radiation exposure of the heart with a dose of 8 Gy, a total number of 731 endothelial proteins were identified, of which 501 proteins contained labelled peptides. 436 proteins were quantified using the statistical criteria described in Methods. Among the quantified proteins, 89 proteins were significantly differentially expressed in irradiated samples compared to controls (±1.3-fold). The abundance of 45 proteins was decreased and that of 44 increased.

After irradiation with a dose of 16 Gy, 578 proteins were identified, of which 389 proteins contained labelled peptides. Quantification of 333 proteins was performed using the

statistical criteria described in the Methods section. Ninety-five proteins were considered as significantly differentially expressed in irradiated samples compared to controls (±1.3-fold); the expression of 49 proteins was down-regulated and that of 46 proteins up-regulated.

Twenty-six significantly deregulated proteins were shared between the two doses representing a general radiation response signature (Table 1). Of these proteins, 13 were up- and 13 down-regulated. The majority of these proteins were involved in cytoskeletal organisation or metabolic activity. Importantly, the direction of deregulation was similar at both doses for all shared proteins.

Bioinformatics analysis revealed cell-cell junction and metabolism pathways affected by irradiation

To understand the protein networks involved in the radiation response, the significantly deregulated proteins were analysed using the STRING software (http://string-db.org). The analysis of both protein profiles showed five distinct but interconnected clusters of proteins: cytoskeletal structure, translation and transcription, heat shock proteins, mitochondrial respiratory chains, and metabolism (Figure 3 A and 3 B).

A detailed analysis of the functional interactions and biological pathways was performed using IPA software (http://www.INGENUITY.com). The analysis showed that networks "inflammatory response", "cellular assembly and organisation" and "DNA replication and repair" were the most altered in the endothelial proteome after 8 Gy (Table S6). The most influenced networks at 16 Gy were "energy production" and "cell-to-cell signalling and interaction", and "cellular movement, assembly and organisation" (Table S7). The most significant protein interaction networks after 8 or 16 Gy were merged to elucidate the central regulatory radiation-responsive nodes; these merged networks are shown in the supporting information, Figure S1 (8 Gy) and Figure S2 (16 Gy). Such nodes that were present at both doses included phosphatidylinositol-4,5-bisphosphate 3-kinase (PI3K), protein kinase (Akt) and extracellular signal regulated kinase (ERK). The pathways "remodelling adherens junction", and "cell-cell junction" were significantly affected after both exposures (Tables S6).

and S7). The alteration in energy metabolism was more pronounced in 16 Gy-exposed samples.

Compiling of the 20 most important canonical pathways of the significantly deregulated proteins provided several overlapping and interconnected super pathways mainly involved in cell communication and cytoskeletal organisation (Figure S3A and Figure S3B). The IPA predicted that insulin receptor (INSR), insulin-like growth factor 1 receptor (IGF1R) and peroxisome proliferator-activated receptor (PPAR) alpha were deactivated after both exposures (Tables S6 and S7). PPAR gamma was predicted to be inhibited only after 16 Gy. The analysis predicted that the myocardin-like 2 (MKL) protein was activated after 8 Gy while MAPK4 and IFNG were activated in the 16 Gy irradiated cardiac endothelial cells (Tables S6 and S7). The analysis indicated interaction between two putative up-stream transcription regulators, namely INSR and IGFR1, based on the shared affected target proteins (Figure 4 A and 4 B). IPA analysis of the differently expressed proteins associated with toxic pathways showed NRF2-mediated oxidative stress response, fatty acid metabolism and mitochondrial dysfunction as the main targets of radiation-induced cellular toxicity after both exposures (Tables S6 and S7). Data analysis indicated a broad range of cardiotoxicity end points including cardiac inflammation, cardiac damage, and cardiac hypertrophy (Tables S6 and S7).

The expression of PI3K cascade genes was affected by irradiation

As PI3K was indicated as a central regulatory radiation-responsive node of the protein networks in our proteome profiling, the alteration in the expression of genes related to PI3K signalling was evaluated. Data for individual genes are provided in Tables S8 and S9. Out of 88 PI3K signalling-related genes examined, 54 and 61 genes showed significant differences $(q^* < 0.03)$ in expression levels between controls, 8 and 16 Gy irradiated mice, respectively (Tables S8 and S9). The expression of most genes belonging to the PI3K signalling pathway was reduced by irradiation (Tables S8 and S9). The analysis showed 50 shared genes the expression of which was altered in both irradiated samples in the same direction. The shared

genes are presented in the bold italic in the Tables S8 and S9. The gene expression of several isoforms of Pi3k, Eif (eukaryotic translation initiation factor), Mapk (mitogen-activated protein kinase kinase), PrKcb (protein kinase C) and Igf1r (insulin-like growth factor I receptor) was reduced in the irradiated cells after both exposures compared to control cells $(q^* < 0.03)$ (Tables S8 and S9).

The irradiation altered genes involved in endothelial senescence

We have previously shown that PI3K signalling pathway is associated with endothelial senescence triggered by chronic low-dose-rate exposure. $^{29, 30}$ To investigate the involvement of senescence after acute high-dose radiation exposure, the expression of genes involved in cellular senescence was analysed. Data for individual genes are provided in Tables S10 and S11. Out of 88 senescence-related genes examined, 25 and 43 genes showed significant differences (q^* < 0.02) in expression levels between controls and 8- or 16 Gy- irradiated mice, respectively (Tables S10 and S11). The analysis showed 24 shared genes the expression of which was altered in both irradiated samples in the same direction. The shared genes are shown in bold italic in the Tables S10 and S11. The gene expression of classical senescence markers such as p21, p16, and lgfbp3 was increased whereas PrKcd (protein kinase C delta) was decreased after both exposures compared to control cells. The gene expression of Nox4 (NADPH oxidase 4) was altered only after 8 Gy (q^* < 0.02) (Tables S10 and S11).

Insulin / IGF signalling pathways were impaired after irradiation

To confirm the deregulation in insulin / IGF cascade, we examined the EC lysates by immunoblotting using antibodies relevant for this pathway. Our gene expression analysis showed that the expression level of Igfr1 gene was reduced after both doses. In addition, the amount of phospho-INSR/ IGF1R was decreased in the irradiated samples compared to the control samples (Figure 5 A and 5 C, p<0.05). The levels of PI3K and phospho-PI3K were reduced in the irradiated samples (Figure 5). No significant change was observed in

the level of AKT but phospho-AKT showed significant reduction in the irradiated samples (Figure 5). The expression level of both mTOR and phospho-mTOR was reduced significantly after 16 Gy (Figure 5). The antibody detection of the key downstream proteins of PI3K pathway such as GSK3 and FOXO3 confirmed the radiation-responsive downregulation of the phosphorylated forms of these proteins (Figure 5 A and 5 C; p<0.05). The immunoblotting showed significantly reduced levels of eNOS and phospho-eNOS in irradiated samples. The analysis showed decreased glucose transporter type 4 (Glut4) content after 16 Gy (Figure 5 ; p<0.05). The analysis indicated less active insulin/IGF-PI3K-Akt signalling pathway after radiation (Figure 5 D).

We also analysed phosphorylation status of the proteins of insulin/MAPK cascade (ERK 44/42 and p38). A significant decrease in abundance was seen for ERK 44/42 in 16 Gy-irradiated samples (Figure 6 A and 6 C; p<0.05). Radiation reduced phosphorylation of ERK 44/42 but increased phosphorylation of p38 (Figure 6 A and 6 D; p<0.05); the level of non-phosphorylated form of p38 did not change after irradiation (Figure 6 A and 6 C; p<0.05). The analysis indicated that ionising radiation affected insulin/IGF-MAPK signalling pathway (Figure 6 D).

Our proteome profiling predicted less capacity of anti-oxidative stress defence Therefore, the protein levels of SOD1, Hsp90 and Hsp70 were analysed. Immunoblot analysis confirmed the markedly decreased level of SOD1 and Hsp90 and increased level of Hsp70 in the irradiated samples (Figure 6 B and 6 E; p<0.05).

To confirm the senescence gene array analysis, the protein expression levels of p16, p21 and p53 were investigated. The antibody detection of senescence markers confirmed the radiation-responsive up-regulation of p16 and p21 found in the gene array analysis (Figure 6 B and 6 F; p<0.05). Immunoblotting did not show any detectable changes in the level of p53 or phospho-p53 after irradiation (Figure 6 B and 6 F; p<0.05).

Irradiation changed IRS serine and tyrosine phosphorylation status

The homeostasis in the phosphorylation level of insulin receptor substrate 1 (IRS-1) plays an important role in the insulin cascade. The endothelial cell lysates were analysed using phospho-IRS-1 (Ser-621, Ser-307 and tyrosines) Sandwich ELISA kits and the data were compared to the level of total IRS-1. Irradiation significantly increased phosphorylation of IRS-1 at Ser-307 and decreased phosphorylation of IRS-1 at tyrosine residues (Figure 7 C and 7 D; p<0.05). The level of total IRS-1 and phospho-IRS1 (Ser-621) did not change after irradiation (Figure 7 A and 7 B; p<0.05).

Endothelial proteins underwent stress modifications after irradiation

The proteomics data indicated the presence of radiation-induced oxidative stress. To confirm this observation, the levels of stress-induced protein modifications including nitrosylation modification and malondialdehyde modification (lipid peroxidation marker) and homocysteinylation were analysed (Figure 8). Significant increase in the level of malondialdehyde-modified proteins, nitrated proteins, homocysteinylated proteins and carbonylated proteins (Figure 8 A, 8 B, 8 C and 8 D; p<0.05) was found after irradiation suggesting protein damage by oxidative stress.

Irradiation enhanced serum inflammation and impaired NO production

As the endothelial dysfunction results in an alteration in serum NO level, 41 the serum of control and irradiated mice was tested. The levels of NO were significantly reduced in the irradiated samples in comparison to controls (Figure 9 A, p<0.05).

Since the endothelial dysfunction is associated with circulating levels of the oxLDL, 42 we compared the level of serum oxLDL in control and irradiated animals. The level of serum oxLDL was significantly higher in the irradiated mice compared to controls (Figure 9 B, p<0.05).

Endothelial dysfunction is also associated with hyperglycemia. ⁴³ We measured the serum glucose levels in control and irradiated animals. The glucose concentration was slightly but

significantly higher in the serum of irradiated animals after 16 Gy than in the controls (Figure 9 C, p<0.05).

To measure the inflammatory response after radiation exposure, we analysed the level of six different cytokines in serum. The serum level of TNF-alpha, IL-1 alpha and IL-6 was significantly increased in the irradiated mice in comparison to controls (Figure 9 D, p<0.05).

Vascular E-selectin was mildly increased in heart sections after irradiation

The morphological changes in the irradiated cardiac vasculature were analysed using immunohistochemistry. Analysis showed a subtle increase in E-selectin staining in irradiated mice hearts [(averaged score 0 Gy: 3.0; 8 Gy: 4.25; 16 Gy: 3.3); Table S12]. As local heart irradiation of mice is known to decrease microvascular density (MVD) 40 weeks after exposure we analysed the MVD on the heart sections in the present study. No clear differences were detectable in the MVD 16 weeks after irradiation (Figure S4 A and S4 B).

Pathways affected by irradiation in cardiac microvascular ECs

All proteins and genes found significantly up- or downregulated in this study were introduced to the IPA to receive a comprehensive "cross-omics" view of all affected pathways and their interactions. These pathways are shown in Figure S5. The upregulation is indicated with a red and downregulation with a green colour. The greatest alterations are seen in the PI3K and MAPK pathways in the cytosolic fraction and in the senescence in the nucleus.

Discussion

The goal of the present study was to elucidate potential biological mechanisms causing the radiation-induced vascular injury and endothelia dysfunction. For the first time, cardiac microvascular endothelial cells were analysed directly after their isolation from irradiated and non-irradiated hearts. The radiation exposures of 8 and 16 Gy induced large alterations in the endothelial proteome; the corresponding proteins are involved in endothelial dysfunction that is hallmarked by increased senescence, enhanced oxidative stress, inflammation and

NO signalling defect. In the context of cellular radiation response many of these findings are novel, yet not in disagreement with the radiation-induced endothelial impairment of previous *in vivo* and *in vitro* studies. ^{12, 26, 27} These data prompt us to propose that these changes are predictive events that result in vascular damage and increased risk of cardiovascular disease after radiation exposure.

Endothelial dysfunction is described as the first pathogenic event of vascular damage. Endothelial barrier dysfunction and cell-cell adhesion and junction impairment are characteristic responses of the endothelium to increasing oxidative stress. 14. The proteome profiling of this study emphasises radiation-induced alterations in endothelial cellular assembly and organisation. Accordingly, we observed alteration in proteins involved in the cytoskeletal organisation and focal adhesion such as actin, tubulin, vimentin and intercellular adhesion molecules (ICAM). Surface marker as well as proteomic analyses demonstrate an increase in the level of ICAM-1 and ICAM-2 after radiation exposure, in agreement with previous data. 44 Increased expression of these adhesion molecules induces endothelial junction alterations and subsequently endothelial cell leakiness. 45 ICAM-1 mediates signal transduction to initiate several pro-inflammatory signalling cascades. 46 ICAM-2 is involved in the leukocyte migration trough the endothelium in response to inflammatory stimuli. 47 Our data also indicate an increase in the level of the cytokine-induced adhesion molecule Eselectin, further suggesting an alteration in microvascular integrity and permeability. 48 Highdose ionising radiation has been shown previously to enhance the gene expression level of E-selectin in cardiac endothelial cells. 49 The increased expression of cadherin, clathrin and catenin after irradiation found in this study further suggests alteration in endothelial permeability but also activation of RhoGTPase signalling. 50

Deficient NO bioavailability is a hallmark of endothelial cell dysfunction that results in impaired endothelium-dependent vasodilation. ⁵¹ Our data indicate a marked decrease of NO levels in the serum of animals after exposure to 8 and 16 Gy. Our immunoblotting data show that the expression level of the active form of eNOS was reduced in irradiated ECs. The radiation-induced impairment of the NO pathway is characteristic of radiation-induced

vascular endothelial injury. ⁵² The loss of NO generation is also associated with accelerated NO degradation by reactive oxygen species (ROS). ⁵³ Peroxynitrite, a product of ROS and NO reaction, increases the level of oxidative and nitrosative stress. ⁵⁴ Consistent with this, we detected considerable changes in the level of stress-induced modifications including lipid peroxidation, protein carbonylation, nitrosylation and homocysteinylation in irradiated ECs. Stress-induced protein modifications precede increased protein degradation or inactivation. ¹⁰ Elevated levels of homocysteine are associated with various human cardiovascular diseases including atherosclerosis. ⁵⁵ Cellular and extracellular protein homocysteinylation causes endothelial dysfunction, ⁵⁶ oxidation of LDL, ⁵⁵ increase in the expression of adhesion molecules on the endothelial cell surface, ⁵⁷ enhanced monocyte adhesion to the vessel wall

Radiation-induced ROS production is accompanied by reduced cellular oxidative capacity. ⁶⁰ The pathway analysis predicted less activation of NFE2L2 transcription factors after both doses, suggesting a reduced capacity of antioxidant defence. ⁶¹ Our data show that the gene and protein levels of SOD1 were reduced after irradiation. In addition, radiation exposure induced alterations in the expression level of other proteins involved in oxidative stress response such as heat shock proteins (Hsp90, Hsp70, and Hsp40), and peroxiredoxin 1. Enhanced ROS production is associated with the disruption of actin filaments ⁶² changing the cellular permeability. ⁶³ Our data also indicate significantly increased levels of oxidised low density lipoprotein (oxLDL) that is a marker of oxidative stress. It contributes in vascular damage including disruption of the endothelial cell barrier, and impairment of NO production.

Our serum cytokine profiling indicated significantly increased levels of TNF alpha, IL-1 alpha and IL-6. Enhanced levels of circulating inflammatory markers have been correlated with endothelial dysfunction, ⁶⁵ impaired insulin signalling, ⁶⁶ reduced bioavailability of NO ⁵³ and vascular ageing ²¹. The pathway analysis predicts a radiation-associated inhibition of PPAR alpha and PPAR gamma suggesting increased inflammation. ⁶⁷ Elevated levels of TNF alpha, ⁶⁸ IL1 and IL-6 ⁶⁹ have been reported in age-associated vascular disease. Both local

and systemic inflammatory response in heart tissue has been shown to alter the endothelial barrier and result in vascular dysfunction. ⁷⁰

Increased ROS also induces a series of signalling mechanisms associated with changes in protein kinase and phosphatase activities that are known to influence the endothelial function. ¹⁴ In this study, marked changes in the phosphorylation status of MAP kinase proteins including ERK44/42 and p38 were found in the irradiated samples. The activation of vascular p38 is observed in heart failure ⁷¹ and it contributes to impaired NO production and vasodilation. ⁷²

The functional correlation analysis of the differentially expressed proteins in the present study predicted the inactivation of the INSR/ IGFR1 after irradiation. In accordance, IGF1-R and INSR showed reduced levels of gene expression and active protein after irradiation. Impaired insulin signalling is a constituent of metabolic disorder and characteristic of endothelial dysfunction. ⁷³ Since eNOS is a downstream protein of the insulin cascade, impairment of endothelial NO production has been described as a link between defective insulin signalling pathway and endothelial dysfunction ⁵³ The balance between PI3K-dependent insulin signalling and MAPK-dependent insulin signalling pathways seems to regulate the main endothelial functions, namely vasodilation and vasoconstriction. ¹⁸

One of the main pathological mechanisms involved in the deactivation of the insulin pathway is lipotoxicity. ⁵³ Mitochondrial dysfunction and subsequently elevated free fatty acid concentrations are typically associated with defective insulin signalling. ⁷⁴ We have previously shown markedly enhanced levels of circulating free fatty acids (FFA) in serum of animals after local irradiation of the heart. ¹⁰In the present study, we found significant alterations in proteins involved in endothelial energy production and oxidative phosphorylation (OXPHOS). It is proposed that persistence exposure of cells to high concentration of FFA activates the serine/threonine kinase cascade and increase phosphorylation of insulin receptor substrates (IRS-1 and IRS-2) on serine/threonine but not at tyrosine sites. Misbalance in IRS serine and tyrosine phosphorylation reduces the ability of the insulin receptor substrates to activate NO production. ⁵³ In a good agreement with this,

our assay of phosphorylation status of IRS confirmed the increase in IRS1 serine phosphorylation but not in tyrosine residues.

An additional mechanism resulting in insulin pathway impairment is hyperglycemia. Impaired INSR/ IGFR1 cascade affects the uptake of glucose due to reduced glucose transporter type 4 translocation to the cell surface. ⁵³ We accordingly observed an increase in serum glucose and a reduction in the Glut4 content. Lower Glut4 level was observed in the context of contractility dysfunction and in excess of FFA in rats. 75 High glucose concentration contributes to endothelial dysfunction ⁵³ and endothelial senescence. ⁷⁶ Hyperglycaemia is also associated with the increased mitochondrial ROS production. 77 The mechanisms of endothelial dysfunction and insulin pathway impairment share many similar features. It has been shown that PI3K-Akt-NO pathway is involved in the glucose uptake and translocation of Glut4 to cell surface in different cell types including cardiomyocytes 78 and adipocytes. 79 Interestingly, it has been reported that administration of chemo-radiation for head and neck carcinoma alters glucose metabolism during and after treatment. 80 A main event of insulin cascade inhibition in endothelial cells is deactivation of in PI3K-Akt pathway.⁵³ Our immunoblotting data and gene expression profiling confirmed that total and active forms of different components of the PI3K-Akt pathway were changed after irradiation. It has been shown that an inhibition of the insulin / IGF1R pathway caused an altered phosphorylation and activation of Akt 81 and mTOR complexes (mTORC1/2) 82 and other downstream targets including Foxo3 83 and GSK3. 84 GSK3 serves as negative regulator of insulin and impairs insulin cascade via IRS1 serine phosphorylation. 85

We have shown before that the PI3K-Akt-mTOR pathway is associated with progression of premature senescence *in vitro* after chronic radiation exposure. ³⁰ Cellular senescence contributes to the endothelial dysfunction *in vivo* and *in vitro*. ⁸⁶ Endothelial senescence is associated with endothelial dysfunction, disrupted cell-cell junctions and increased monolayer permeability. ⁸⁷ Our data show an increase in the senescent markers of irradiated cells including accumulation of p21 and p16, ^{88, 89} increased amount of cadherin, ⁸⁷ and ICAM, ⁹⁰ and reduced level of prohibitin-1. ⁹¹ High acute doses of ionising radiation have

been shown to induce a senescence-like phenotype in endothelial cells with a significant decrease in angiogenic activity in vitro 92 and in vivo. 93 Persistent up-regulation of senescence marker expression has been observed in vivo after irradiation. ⁹⁴ Recently, Panganiban and Day have shown that high dose radiation (10 Gy X-ray) induced IGF1R phosphorylation 24h after exposure in human pulmonary arterial endothelial cells (HPAEC). 95 The authors suggested that the activation of IGF1R contributed to accelerated senescence in these cells. Although our study and that of Panganiban and Day both investigated the effect of irradiation on endothelial senescence, a direct comparison between the studies is difficult. The study by Panganiban and Day was performed on primary lung endothelial cells that were in vitro irradiated and analysed shortly after the exposure. 95 In contrast, we analysed freshly harvested primary endothelial cells from in vivo irradiated hearts 16 weeks after exposure. The nature of stress-induced accelerated senescence differs in in vivo and in vitro environments. The isolated cardiac endothelial cells in our study were a target of a complex cellular communication and exposed to local and circulatory stress-induced molecules. However, both studies emphasise the important role of IGF11R in the radiation-induced endothelial senescence.

In addition to deactivation of insulin / IGF1R pathway, the endothelial proteome profiling in this study predicts an inhibition of the transcription factor PPAR alpha after irradiation. We have previously shown that high-dose radiation altered the cardiac fatty acid oxidation and increased inflammation due to the impairment of the PPAR alpha transcription factor activity.

The members of the PPAR family are expressed in endothelial cells and play a role in endothelial cell function and structure.

Endothelial PPAR alpha regulates mainly the leukocyte recruitment and adhesion to endothelial cells,

reduction,

inflammatory signalling,

and regulation of oxLDL-dependent pathway by alteration in cellular lipids.

Repart alpha ligands are shown to stimulate eNOS expression.

Furthermore, a negative correlation between PPAR alpha activity and the level of homocysteine has been reported.

PPARs are involved in the endothelial FFA transport by regulating the fatty acid binding

proteins. ¹⁰¹ A decrease in the level of the fatty acid binding protein 4 (FABP4) and reduced fatty acid oxidation in the endothelial cell proteome after was observed after 16 Gy irradiation. Our immunoblotting data showed enhanced levels of active (less phosphorylated) form of GSK3 beta after irradiation. The active GSK3 has been shown to phosphorylate PPAR alpha and thereby increase its turn-over and ubiquitination. ¹⁰² GSK3 beta is activated by inflammation and associated with increased endothelial adhesion molecule expression. ¹⁰³ Our data emphasise the role of PPAR alpha in heart pathophysiology after high-dose radiation where impairment of PPAR may orchestrate the myocardial and endothelial pathology.

Taken together, the data gathered here using different methods strongly suggest a radiation-dependent inactivation of both insulin-dependent PI3K and MAPK signalling pathways. A putative model of the role of these pathways in radiation-induced cardiovascular damage is presented in Figure 10. It proposes that irradiation deactivates the insulin signalling in endothelial cells via the insulin receptor substrate-PI3K-Akt pathway to reduce the activation of endothelial nitric-oxide synthase (eNOS). The event is accompanied by alteration in MAPK cascade and followed by increased oxidative stress and inflammation confirming earlier observations of a pro-inflammatory reaction of endothelial cells to irradiation. Elevated levels of FFA and glucose alter the homeostasis of insulin receptor substrate serine / tyrosine phosphorylation and change the activity of the insulin receptor. Deactivation of the insulin/IGF-PI3K-Akt cascade is characterised by a low level of NO bioavailability, increased ROS production, enhanced endothelial permeability and adhesion, endothelial senescence, and elevated circulatory cytokines. These changes are proposed to contribute in endothelial dysfunction and vascular injury after radiation exposure.

Clinical application

Endothelial dysfunction has been described as an early and critical marker of response to irradiation.

Further, EC dysfunction has been qualified as a marker of cardiovascular disease. ¹³ European hypertension guidelines ¹⁰⁴ recognised endothelial cell function as a therapeutic target to reduce cardiovascular risk. ¹⁰⁵ Screening of endothelial function in a reliable and cost-effective manner could be applied for future cardiovascular therapy. The upstream regulators and mediators of PI3K pathway such as PPAR alpha and IGF need to be considered as future therapeutic targets protecting the patient from vascular complications due to radiotherapy.

Supporting information,

Supporting information, including supplementary figures and tables to this article is available free of charge via http://pubs.acs.org/.

Supplementary Figures:

- Fig. S1. Graphical representation of the merged most significant protein interaction networks after 8 Gy using Ingenuity Pathway Analysis of differentially regulated proteins.
- Fig. S2. Graphical representation of the merged most significant protein interaction networks after 16 Gy using Ingenuity Pathway Analysis of differentially regulated proteins.
- Fig. S3. Graphical representation of 20 most important canonical pathway networks representing significantly deregulated proteins after 8 Gy (A) and 16 Gy (B) (http://www.INGENUITY.com).
- Fig. S4. The analysis of endothelial E-selectin expression (A) and myocardial microvessel density (MDV) using CD31 immunohistochemistry (B).
- Fig. S5. Graphical representation of mainly molecular network affected in cardiac microvascular endothelial cells after 8 Gy (A) and 16 Gy (B).

Supplementary Tables:

- Table S1. H/L fold change ratio of the spiked proteins quantified by ICPL approach.
- Table S2. Significantly differently expressed proteins quantified by ICPL approach after 8 Gy exposure.
- Table S3. Significantly differently expressed proteins quantified by ICPL approach after 16 Gy exposure.

Table S4. All peptides identified and quantified by ICPL approach after 8 Gy exposure.

Table S5. All peptides identified and quantified by ICPL approach after 16 Gy exposure.

Table S6. IPA Analysis summary of significantly deregulated proteins after 8 Gy exposure.

Table S7. IPA Analysis summary of significantly deregulated proteins after 16 Gy exposure.

Table S8. The Mouse PI3K signalling Targets RT² Profiler PCR Array profile after 8 Gy exposure

Table S9.The Mouse PI3K signallingTargets RT² Profiler PCR Array profile after 16 Gy exposure

Table S10.The mouse senescence targets RT² Profiler PCR Array profile after 8 Gy exposure

Table S11.The mouse senescence targets RT² Profiler PCR Array profile after 16 Gy exposure

Table S12. The analysis of myocardial microvessel density (MDV) using CD31 immunohistochemistry and evaluation of endothelial E-selectin expression

Acknowledgements

We thank Stefanie Winkler and Sandra Helm for excellent technical assistance. The study was funded by the DFG SFB824/B4, INST95/980-1 FUGG, INST411/37-1FUGG, BMBF Kompetenzverbund Strahlenforschung and BMBF m4 Verbund Personalisierte Medizin (16GW0030).

The authors declare no competing financial interest.

References

1. Swerdlow, A. J.; Higgins, C. D.; Smith, P.; Cunningham, D.; Hancock, B. W.; Horwich, A.; Hoskin, P. J.; Lister, A.; Radford, J. A.; Rohatiner, A. Z.; Linch, D. C.,

Myocardial infarction mortality risk after treatment for Hodgkin disease: a collaborative British cohort study. *J Natl Cancer Inst* **2007**, 99, (3), 206-14.

- 2. Darby, S. C.; Ewertz, M.; McGale, P.; Bennet, A. M.; Blom-Goldman, U.; Bronnum, D.; Correa, C.; Cutter, D.; Gagliardi, G.; Gigante, B.; Jensen, M. B.; Nisbet, A.; Peto, R.; Rahimi, K.; Taylor, C.; Hall, P., Risk of ischemic heart disease in women after radiotherapy for breast cancer. *N Engl J Med* **2013**, 368, (11), 987-98.
- 3. Carr, Z. A.; Land, C. E.; Kleinerman, R. A.; Weinstock, R. W.; Stovall, M.; Griem, M. L.; Mabuchi, K., Coronary heart disease after radiotherapy for peptic ulcer disease. *Int J Radiat Oncol Biol Phys* **2005**, 61, (3), 842-50.
- 4. Tukenova, M.; Guibout, C.; Oberlin, O.; Doyon, F.; Mousannif, A.; Haddy, N.; Guerin, S.; Pacquement, H.; Aouba, A.; Hawkins, M.; Winter, D.; Bourhis, J.; Lefkopoulos, D.; Diallo, I.; de Vathaire, F., Role of cancer treatment in long-term overall and cardiovascular mortality after childhood cancer. *J Clin Oncol* **2010**, 28, (8), 1308-15.
- 5. Wondergem, J.; Boerma, M.; Kodama, K.; Stewart, F. A.; Trott, K. R., Cardiovascular effects after low-dose exposure and radiotherapy: what research is needed? *Radiat Environ Biophys* **2013**, 52, (4), 425-34.
- 6. Taylor, C. W.; Povall, J. M.; McGale, P.; Nisbet, A.; Dodwell, D.; Smith, J. T.; Darby, S. C., Cardiac dose from tangential breast cancer radiotherapy in the year 2006. *Int J Radiat Oncol Biol Phys* **2008**, 72, (2), 501-7.
- 7. Boerma, M.; Hauer-Jensen, M., Preclinical research into basic mechanisms of radiation-induced heart disease. *Cardiol Res Pract* **2010**, 2011.
- 8. Baker, J. E.; Fish, B. L.; Su, J.; Haworth, S. T.; Strande, J. L.; Komorowski, R. A.; Migrino, R. Q.; Doppalapudi, A.; Harmann, L.; Allen Li, X.; Hopewell, J. W.; Moulder, J. E., 10 Gy total body irradiation increases risk of coronary sclerosis, degeneration of heart structure and function in a rat model. *Int J Radiat Biol* **2009**, 85, (12), 1089-100.
- 9. Baker, J. E.; Moulder, J. E.; Hopewell, J. W., Radiation as a risk factor for cardiovascular disease. *Antioxid Redox Signal* **2011**, 15, (7), 1945-56.
- 10. Azimzadeh, O.; Sievert, W.; Sarioglu, H.; Yentrapalli, R.; Barjaktarovic, Z.; Sriharshan, A.; Ueffing, M.; Janik, D.; Aichler, M.; Atkinson, M. J.; Multhoff, G.; Tapio, S., PPAR Alpha: A Novel Radiation Target in Locally Exposed Mus musculus Heart Revealed by Quantitative Proteomics. *J Proteome Res* **2013**, 12, (6), 2700-14.
- 11. Gabriels, K.; Hoving, S.; Seemann, I.; Visser, N. L.; Gijbels, M. J.; Pol, J. F.; Daemen, M. J.; Stewart, F. A.; Heeneman, S., Local heart irradiation of ApoE (-/-) mice induces microvascular and endocardial damage and accelerates coronary atherosclerosis. *Radiother Oncol* **2012**, 105, (3), 358-64.

- 12. Seemann, I.; Gabriels, K.; Visser, N. L.; Hoving, S.; te Poele, J. A.; Pol, J. F.; Gijbels, M. J.; Janssen, B. J.; van Leeuwen, F. W.; Daemen, M. J.; Heeneman, S.; Stewart, F. A., Irradiation induced modest changes in murine cardiac function despite progressive structural damage to the myocardium and microvasculature. *Radiother Oncol* **2012**, 103, (2), 143-50.
- 13. Kolluru, G. K.; Bir, S. C.; Kevil, C. G., Endothelial dysfunction and diabetes: effects on angiogenesis, vascular remodeling, and wound healing. *Int J Vasc Med* **2012**, 2012, 918267.
- 14. Lum, H.; Roebuck, K. A., Oxidant stress and endothelial cell dysfunction. *Am J Physiol Cell Physiol* **2001**, 280, (4), C719-41.
- 15. Zeng, G.; Nystrom, F. H.; Ravichandran, L. V.; Cong, L. N.; Kirby, M.; Mostowski, H.; Quon, M. J., Roles for insulin receptor, PI3-kinase, and Akt in insulin-signaling pathways related to production of nitric oxide in human vascular endothelial cells. *Circulation* **2000**, 101, (13), 1539-45.
- 16. Montagnani, M.; Ravichandran, L. V.; Chen, H.; Esposito, D. L.; Quon, M. J., Insulin receptor substrate-1 and phosphoinositide-dependent kinase-1 are required for insulin-stimulated production of nitric oxide in endothelial cells. *Mol Endocrinol* **2002,** 16, (8), 1931-42.
- 17. Formoso, G.; Chen, H.; Kim, J. A.; Montagnani, M.; Consoli, A.; Quon, M. J., Dehydroepiandrosterone mimics acute actions of insulin to stimulate production of both nitric oxide and endothelin 1 via distinct phosphatidylinositol 3-kinase- and mitogen-activated protein kinase-dependent pathways in vascular endothelium. *Mol Endocrinol* **2006**, 20, (5), 1153-63.
- 18. Muniyappa, R.; Sowers, J. R., Role of insulin resistance in endothelial dysfunction. *Rev Endocr Metab Disord* **2013**, 14, (1), 5-12.
- 19. Hopewell, J. W.; Calvo, W.; Jaenke, R.; Reinhold, H. S.; Robbins, M. E.; Whitehouse, E. M., Microvasculature and radiation damage. *Recent Results Cancer Res* **1993**, 130, 1-16.
- 20. Wang, J.; Boerma, M.; Fu, Q.; Hauer-Jensen, M., Significance of endothelial dysfunction in the pathogenesis of early and delayed radiation enteropathy. *World J Gastroenterol* **2007**, 13, (22), 3047-55.
- 21. El Assar, M.; Angulo, J.; Rodriguez-Manas, L., Oxidative stress and vascular inflammation in aging. *Free Radic Biol Med* **2013**, 65, 380-401.
- 22. Schofield, P. N.; Garcia-Bernardo, J., Radiation, oxidative stress and senescence; the vascular endothelial cell as a common target? In *Multiple Stressors: A Challenge for the Future*, Mothersill, C.; Mosse, I.; Seymour, C., Eds. Springer: Netherlands, 2007; Vol. 4, pp 325-334

- 23. AGIR, Circulatory Disease Risk. Report on the Independent Advisory Group on Ionising Radiation. *Health Protection Agency.*
- http://www.hpa.org.uk/Publications/Radiation/DocumentsOfTheHPA/RCE16CirculatoryDiseaseRisk/2010.
- 24. Darby, S. C.; Cutter, D. J.; Boerma, M.; Constine, L. S.; Fajardo, L. F.; Kodama, K.; Mabuchi, K.; Marks, L. B.; Mettler, F. A.; Pierce, L. J.; Trott, K. R.; Yeh, E. T.; Shore, R. E., Radiation-related heart disease: current knowledge and future prospects. *Int J Radiat Oncol Biol Phys* **2010**, 76, (3), 656-65.
- 25. Seemann, I.; Te Poele, J. A.; Hoving, S.; Stewart, F. A., Mouse bone marrow-derived endothelial progenitor cells do not restore radiation-induced microvascular damage. *ISRN Cardiol* **2014**, 2014, 506348.
- 26. Pluder, F.; Barjaktarovic, Z.; Azimzadeh, O.; Mortl, S.; Kramer, A.; Steininger, S.; Sarioglu, H.; Leszczynski, D.; Nylund, R.; Hakanen, A.; Sriharshan, A.; Atkinson, M. J.; Tapio, S., Low-dose irradiation causes rapid alterations to the proteome of the human endothelial cell line EA.hy926. *Radiat Environ Biophys* **2011**, 50, (1), 155-66.
- 27. Sriharshan, A.; Boldt, K.; Sarioglu, H.; Barjaktarovic, Z.; Azimzadeh, O.; Hieber, L.; Zitzelsberger, H.; Ueffing, M.; Atkinson, M. J.; Tapio, S., Proteomic analysis by SILAC and 2D-DIGE reveals radiation-induced endothelial response: Four key pathways. *J Proteomics* **2012**, 75, (8), 2319-30.
- 28. Sriharshan, A.; Kraemer, A.; Atkinson, M. J.; Moertl, S.; Tapio, S., Radiation-induced crosstalk between microRNAs and proteins of the endothelium: in silico analysis. *J Proteomics Bioinform* **2014,** 7, (10), 327-331.
- 29. Yentrapalli, R.; Azimzadeh, O.; Barjaktarovic, Z.; Sarioglu, H.; Wojcik, A.; Harms-Ringdahl, M.; Atkinson, M. J.; Haghdoost, S.; Tapio, S., Quantitative proteomic analysis reveals induction of premature senescence in human umbilical vein endothelial cells exposed to chronic low-dose rate gamma radiation. *Proteomics* **2013**, 13, (7), 1096-107.
- 30. Yentrapalli, R.; Azimzadeh, O.; Sriharshan, A.; Malinowsky, K.; Merl, J.; Wojcik, A.; Harms-Ringdahl, M.; Atkinson, M. J.; Becker, K. F.; Haghdoost, S.; Tapio, S., The PI3K/Akt/mTOR Pathway Is Implicated in the Premature Senescence of Primary Human Endothelial Cells Exposed to Chronic Radiation. *PLoS One* **2013**, 8, (8), e70024.
- 31. Sievert, W.; Tapio, S.; Breuninger, S.; Gaipl, U.; Andratschke, N.; Trott, K. R.; Multhoff, G., Adhesion molecule expression and function of primary endothelial cells in benign and malignant tissues correlates with proliferation. *PLoS One* **2014,** 9, (3), e91808.
- 32. Azimzadeh, O.; Scherthan, H.; Sarioglu, H.; Barjaktarovic, Z.; Conrad, M.; Vogt, A.; Calzada-Wack, J.; Neff, F.; Aubele, M.; Buske, C.; Atkinson, M. J.; Tapio, S., Rapid

proteomic remodeling of cardiac tissue caused by total body ionizing radiation. *Proteomics* **2011,** 11, (16), 3299-311.

- 33. Merl, J.; Ueffing, M.; Hauck, S. M.; von Toerne, C., Direct comparison of MS-based label-free and SILAC quantitative proteome profiling strategies in primary retinal Muller cells. *Proteomics* **2012**, 12, (12), 1902-11.
- 34. Brosch, M.; Yu, L.; Hubbard, T.; Choudhary, J., Accurate and sensitive peptide identification with Mascot Percolator. *J Proteome Res* **2009**, 8, (6), 3176-81.
- 35. Papaioannou, M. D.; Lagarrigue, M.; Vejnar, C. E.; Rolland, A. D.; Kuhne, F.; Aubry, F.; Schaad, O.; Fort, A.; Descombes, P.; Neerman-Arbez, M.; Guillou, F.; Zdobnov, E. M.; Pineau, C.; Nef, S., Loss of Dicer in Sertoli cells has a major impact on the testicular proteome of mice. *Mol Cell Proteomics* **2011**, 10, (4), M900587MCP200.
- 36. Wu, J.; Liu, W.; Bemis, A.; Wang, E.; Qiu, Y.; Morris, E. A.; Flannery, C. R.; Yang, Z., Comparative proteomic characterization of articular cartilage tissue from normal donors and patients with osteoarthritis. *Arthritis Rheum* **2007**, 56, (11), 3675-84.
- 37. D'Eustachio, P., Reactome knowledgebase of human biological pathways and processes. *Methods Mol Biol* **2011**, 694, 49-61.
- 38. Benjamini, Y.; Hochberg, a. Y., Controlling the False Discovery Rate: A Practical and Powerful Approach to Multiple Testing. *Journal of the Royal Statistical Society, Series B*(Methodological) 1995, 57, (1), 289-300.
- 39. Weidner, N.; Semple, J. P.; Welch, W. R.; Folkman, J., Tumor angiogenesis and metastasis--correlation in invasive breast carcinoma. *N Engl J Med* **1991**, 324, (1), 1-8.
- 40. Tsokos, M.; Fehlauer, F.; Puschel, K., Immunohistochemical expression of E-selectin in sepsis-induced lung injury. *Int J Legal Med* **2000**, 113, (6), 338-42.
- 41. Murray, A. J.; Panagia, M.; Hauton, D.; Gibbons, G. F.; Clarke, K., Plasma free fatty acids and peroxisome proliferator-activated receptor alpha in the control of myocardial uncoupling protein levels. *Diabetes* **2005**, 54, (12), 3496-502.
- 42. Marin, C.; Yubero-Serrano, E. M.; Lopez-Miranda, J.; Perez-Jimenez, F., Endothelial aging associated with oxidative stress can be modulated by a healthy mediterranean diet. *Int J Mol Sci* **2013**, 14, (5), 8869-89.
- 43. Lee, C. H.; Shieh, Y. S.; Hsiao, F. C.; Kuo, F. C.; Lin, C. Y.; Hsieh, C. H.; Hung, Y. J., High glucose induces human endothelial dysfunction through an Axl-dependent mechanism. *Cardiovasc Diabetol* **2014**, 13, (1), 53.
- 44. Kiyohara, H.; Ishizaki, Y.; Suzuki, Y.; Katoh, H.; Hamada, N.; Ohno, T.; Takahashi, T.; Kobayashi, Y.; Nakano, T., Radiation-induced ICAM-1 expression via TGF-beta1 pathway on human umbilical vein endothelial cells; comparison between X-ray and carbonion beam irradiation. *J Radiat Res* **2011**, 52, (3), 287-92.

- 45. Clark, P. R.; Manes, T. D.; Pober, J. S.; Kluger, M. S., Increased ICAM-1 expression causes endothelial cell leakiness, cytoskeletal reorganization and junctional alterations. *J Invest Dermatol* **2007**, 127, (4), 762-74.
- 46. Lawson, C.; Wolf, S., ICAM-1 signaling in endothelial cells. *Pharmacol Rep* **2009**, 61, (1), 22-32.
- 47. Woodfin, A.; Voisin, M. B.; Imhof, B. A.; Dejana, E.; Engelhardt, B.; Nourshargh, S., Endothelial cell activation leads to neutrophil transmigration as supported by the sequential roles of ICAM-2, JAM-A, and PECAM-1. *Blood* **2009**, 113, (24), 6246-57.
- 48. Kim, I.; Moon, S. O.; Park, S. K.; Chae, S. W.; Koh, G. Y., Angiopoietin-1 reduces VEGF-stimulated leukocyte adhesion to endothelial cells by reducing ICAM-1, VCAM-1, and E-selectin expression. *Circ Res* **2001**, 89, (6), 477-9.
- 49. Jelonek, K.; Walaszczyk, A.; Gabrys, D.; Pietrowska, M.; Kanthou, C.; Widlak, P., Cardiac endothelial cells isolated from mouse heart a novel model for radiobiology. *Acta Biochim Pol* **2011**, 58, (3), 397-404.
- 50. Semina, E. V.; Rubina, K. A.; Sysoeva, V. Y.; Rutkevich, P. N.; Kashirina, N. M.; Tkachuk, V. A., Novel mechanism regulating endothelial permeability via T-cadherin-dependent VE-cadherin phosphorylation and clathrin-mediated endocytosis. *Mol Cell Biochem* **2014**, 387, (1-2), 39-53.
- 51. Sugihara, T.; Hattori, Y.; Yamamoto, Y.; Qi, F.; Ichikawa, R.; Sato, A.; Liu, M. Y.; Abe, K.; Kanno, M., Preferential impairment of nitric oxide-mediated endothelium-dependent relaxation in human cervical arteries after irradiation. *Circulation* **1999**, 100, *(*6), 635-41.
- 52. Hong, C. W.; Kim, Y. M.; Pyo, H.; Lee, J. H.; Kim, S.; Lee, S.; Noh, J. M., Involvement of inducible nitric oxide synthase in radiation-induced vascular endothelial damage. *J Radiat Res* **2013**, 54, (6), 1036-42.
- 53. Kim, J. A.; Montagnani, M.; Koh, K. K.; Quon, M. J., Reciprocal relationships between insulin resistance and endothelial dysfunction: molecular and pathophysiological mechanisms. *Circulation* **2006**, 113, (15), 1888-904.
- van der Loo, B.; Labugger, R.; Skepper, J. N.; Bachschmid, M.; Kilo, J.; Powell, J. M.; Palacios-Callender, M.; Erusalimsky, J. D.; Quaschning, T.; Malinski, T.; Gygi, D.; Ullrich, V.; Luscher, T. F., Enhanced peroxynitrite formation is associated with vascular aging. *J Exp Med* **2000**, 192, (12), 1731-44.
- 55. Mujumdar, V. S.; Tummalapalli, C. M.; Aru, G. M.; Tyagi, S. C., Mechanism of constrictive vascular remodeling by homocysteine: role of PPAR. *Am J Physiol Cell Physiol* **2002**, 282, (5), C1009-15.

- 56. Jakubowski, H.; Zhang, L.; Bardeguez, A.; Aviv, A., Homocysteine thiolactone and protein homocysteinylation in human endothelial cells: implications for atherosclerosis. *Circ Res* **2000**, 87, (1), 45-51.
- 57. Brunner, H.; Cockcroft, J. R.; Deanfield, J.; Donald, A.; Ferrannini, E.; Halcox, J.; Kiowski, W.; Luscher, T. F.; Mancia, G.; Natali, A.; Oliver, J. J.; Pessina, A. C.; Rizzoni, D.; Rossi, G. P.; Salvetti, A.; Spieker, L. E.; Taddei, S.; Webb, D. J., Endothelial function and dysfunction. Part II: Association with cardiovascular risk factors and diseases. A statement by the Working Group on Endothelins and Endothelial Factors of the European Society of Hypertension. *J Hypertens* **2005**, 23, (2), 233-46.
- 58. Kaul, S.; Zadeh, A. A.; Shah, P. K., Homocysteine hypothesis for atherothrombotic cardiovascular disease: not validated. *J Am Coll Cardiol* **2006**, 48, (5), 914-23.
- 59. Zhang, X.; Li, H.; Jin, H.; Ebin, Z.; Brodsky, S.; Goligorsky, M. S., Effects of homocysteine on endothelial nitric oxide production. *Am J Physiol Renal Physiol* **2000**, 279, (4), F671-8.
- 60. Zhao, W.; Robbins, M. E., Inflammation and chronic oxidative stress in radiation-induced late normal tissue injury: therapeutic implications. *Curr Med Chem* **2009,** 16, (2), 130-43.
- 61. Tan, Y.; Ichikawa, T.; Li, J.; Si, Q.; Yang, H.; Chen, X.; Goldblatt, C. S.; Meyer, C. J.; Li, X.; Cai, L.; Cui, T., Diabetic downregulation of Nrf2 activity via ERK contributes to oxidative stress-induced insulin resistance in cardiac cells in vitro and in vivo. *Diabetes* **2011**, 60, (2), 625-33.
- 62. Hinshaw, D. B.; Burger, J. M.; Armstrong, B. C.; Hyslop, P. A., Mechanism of endothelial cell shape change in oxidant injury. *J Surg Res* **1989**, 46, (4), 339-49.
- 63. Holman, R. G.; Maier, R. V., Oxidant-induced endothelial leak correlates with decreased cellular energy levels. *Am Rev Respir Dis* **1990**, 141, (1), 134-40.
- 64. Byfield, F. J.; Tikku, S.; Rothblat, G. H.; Gooch, K. J.; Levitan, I., OxLDL increases endothelial stiffness, force generation, and network formation. *J Lipid Res* **2006**, 47, (4), 715-23.
- 65. Csiszar, A.; Labinskyy, N.; Smith, K.; Rivera, A.; Orosz, Z.; Ungvari, Z., Vasculoprotective effects of anti-tumor necrosis factor-alpha treatment in aging. *Am J Pathol* **2007,** 170, (1), 388-98.
- 66. Andreozzi, F.; Laratta, E.; Procopio, C.; Hribal, M. L.; Sciacqua, A.; Perticone, M.; Miele, C.; Perticone, F.; Sesti, G., Interleukin-6 impairs the insulin signaling pathway, promoting production of nitric oxide in human umbilical vein endothelial cells. *Mol Cell Biol* **2007**, 27, (6), 2372-83.

- 67. Smeets, P. J.; Planavila, A.; van der Vusse, G. J.; van Bilsen, M., Peroxisome proliferator-activated receptors and inflammation: take it to heart. *Acta Physiol (Oxf)* **2007**, 191, (3), 171-88.
- 68. Csiszar, A.; Wang, M.; Lakatta, E. G.; Ungvari, Z., Inflammation and endothelial dysfunction during aging: role of NF-kappaB. *J Appl Physiol* (1985) **2008,** 105, (4), 1333-41.
- 69. Ungvari, Z.; Csiszar, A.; Kaley, G., Vascular inflammation in aging. *Herz* **2004,** 29, (8), 733-40.
- 70. Eltzschig, H. K.; Collard, C. D., Vascular ischaemia and reperfusion injury. *Br Med Bull* **2004**, 70, 71-86.
- 71. Widder, J.; Behr, T.; Fraccarollo, D.; Hu, K.; Galuppo, P.; Tas, P.; Angermann, C. E.; Ertl, G.; Bauersachs, J., Vascular endothelial dysfunction and superoxide anion production in heart failure are p38 MAP kinase-dependent. *Cardiovasc Res* **2004**, 63, (1), 161-7.
- 72. Huang, A.; Yang, Y. M.; Yan, C.; Kaley, G.; Hintze, T. H.; Sun, D., Altered MAPK signaling in progressive deterioration of endothelial function in diabetic mice. *Diabetes* **2012**, 61, (12), 3181-8.
- 73. Wiench, B.; Chen, Y. R.; Paulsen, M.; Hamm, R.; Schroder, S.; Yang, N. S.; Efferth, T., Integration of Different "-omics" Technologies Identifies Inhibition of the IGF1R-Akt-mTOR Signaling Cascade Involved in the Cytotoxic Effect of Shikonin against Leukemia Cells. *Evid Based Complement Alternat Med* **2013**, 2013, 818709.
- 74. Shulman, G. I., Cellular mechanisms of insulin resistance. *J Clin Invest* **2000**, 106, (2), 171-6.
- 75. Leguisamo, N. M.; Lehnen, A. M.; Machado, U. F.; Okamoto, M. M.; Markoski, M. M.; Pinto, G. H.; Schaan, B. D., GLUT4 content decreases along with insulin resistance and high levels of inflammatory markers in rats with metabolic syndrome. *Cardiovasc Diabetol* **2012**, 11, 100.
- 76. Zhong, W.; Zou, G.; Gu, J.; Zhang, J., L-arginine attenuates high glucose-accelerated senescence in human umbilical vein endothelial cells. *Diabetes Res Clin Pract* **2010,** 89, (1), 38-45.
- 77. McGill, H. C., Jr.; McMahan, C. A.; Herderick, E. E.; Zieske, A. W.; Malcom, G. T.; Tracy, R. E.; Strong, J. P., Obesity accelerates the progression of coronary atherosclerosis in young men. *Circulation* **2002**, 105, (23), 2712-8.
- 78. Zhu, Y.; Pereira, R. O.; O'Neill, B. T.; Riehle, C.; Ilkun, O.; Wende, A. R.; Rawlings, T. A.; Zhang, Y. C.; Zhang, Q.; Klip, A.; Shiojima, I.; Walsh, K.; Abel, E. D., Cardiac Pl3K-Akt impairs insulin-stimulated glucose uptake independent of mTORC1 and GLUT4 translocation. *Mol Endocrinol* **2013**, 27, (1), 172-84.

- 79. Tanaka, T.; Nakatani, K.; Morioka, K.; Urakawa, H.; Maruyama, N.; Kitagawa, N.; Katsuki, A.; Araki-Sasaki, R.; Hori, Y.; Gabazza, E. C.; Yano, Y.; Wada, H.; Nobori, T.; Sumida, Y.; Adachi, Y., Nitric oxide stimulates glucose transport through insulin-independent GLUT4 translocation in 3T3-L1 adipocytes. *Eur J Endocrinol* **2003**, 149, (1), 61-7.
- 80. Nguyen, N. P.; Vos, P.; Vinh-Hung, V.; Borok, T. L.; Dutta, S.; Karlsson, U.; Lee, H.; Martinez, T.; Jo, B. H.; Nguyen, L. M.; Nguyen, N.; Sallah, S., Altered glucose metabolism during chemoradiation for head and neck cancer. *Anticancer Res* **2009**, 29, (11), 4683-7.
- 81. Pollak, M., The insulin and insulin-like growth factor receptor family in neoplasia: an update. *Nat Rev Cancer* **2012,** 12, (3), 159-69.
- 82. Hsieh, T. C.; Lin, C. Y.; Lin, H. Y.; Wu, J. M., AKT/mTOR as Novel Targets of Polyphenol Piceatannol Possibly Contributing to Inhibition of Proliferation of Cultured Prostate Cancer Cells. *ISRN Urol* **2012**, 2012, 272697.
- 83. Yu, Q.; Gao, F.; Ma, X. L., Insulin says NO to cardiovascular disease. *Cardiovasc Res* **2011**, 89, (3), 516-24.
- 84. Seo, Y. H.; Jung, H. J.; Shin, H. T.; Kim, Y. M.; Yim, H.; Chung, H. Y.; Lim, I. K.; Yoon, G., Enhanced glycogenesis is involved in cellular senescence via GSK3/GS modulation. *Aging Cell* **2008**, 7, (6), 894-907.
- 85. Eldar-Finkelman, H., Glycogen synthase kinase-3--a promising therapeutic target: Dr Hagit Eldar-Finkelman interviewed by Emma Quigley. *Expert Opin Ther Targets* **2006**, 10, (2), 199-201.
- 86. Erusalimsky, J. D.; Kurz, D. J., Endothelial cell senescence. *Handb Exp Pharmacol* **2006**, (176 Pt 2), 213-48.
- 87. Krouwer, V. J.; Hekking, L. H.; Langelaar-Makkinje, M.; Regan-Klapisz, E.; Post, J. A., Endothelial cell senescence is associated with disrupted cell-cell junctions and increased monolayer permeability. *Vasc Cell* **2012**, 4, (1), 12.
- 88. Shelton, D. N.; Chang, E.; Whittier, P. S.; Choi, D.; Funk, W. D., Microarray analysis of replicative senescence. *Curr Biol* **1999**, 9. (17), 939-45.
- 89. Chen, J.; Huang, X.; Halicka, D.; Brodsky, S.; Avram, A.; Eskander, J.; Bloomgarden, N. A.; Darzynkiewicz, Z.; Goligorsky, M. S., Contribution of p16INK4a and p21CIP1 pathways to induction of premature senescence of human endothelial cells: permissive role of p53. *Am J Physiol Heart Circ Physiol* **2006**, 290, (4), H1575-86.
- 90. Minamino, T.; Komuro, I., Role of telomere in endothelial dysfunction in atherosclerosis. *Curr Opin Lipidol* **2002**, 13, (5), 537-43.
- 91. Schleicher, M.; Shepherd, B. R.; Suarez, Y.; Fernandez-Hernando, C.; Yu, J.; Pan, Y.; Acevedo, L. M.; Shadel, G. S.; Sessa, W. C., Prohibitin-1 maintains the angiogenic

- capacity of endothelial cells by regulating mitochondrial function and senescence. *J Cell Biol* **2008**, 180, (1), 101-12.
- 92. Igarashi, K.; Sakimoto, I.; Kataoka, K.; Ohta, K.; Miura, M., Radiation-induced senescence-like phenotype in proliferating and plateau-phase vascular endothelial cells. *Exp Cell Res* **2007**, 313, (15), 3326-36.
- 93. Imaizumi, N.; Monnier, Y.; Hegi, M.; Mirimanoff, R. O.; Ruegg, C., Radiotherapy suppresses angiogenesis in mice through TGF-betaRI/ALK5-dependent inhibition of endothelial cell sprouting. *PLoS One* **2010**, 5, (6), e11084.
- 94. Seol, M. A.; Jung, U.; Eom, H. S.; Kim, S. H.; Park, H. R.; Jo, S. K., Prolonged expression of senescence markers in mice exposed to gamma-irradiation. *J Vet Sci* **2012**, 13, (4), 331-8.
- 95. Panganiban, R. A.; Day, R. M., Inhibition of IGF-1R prevents ionizing radiation-induced primary endothelial cell senescence. *PLoS One* **2013**, 8, (10), e78589.
- 96. Bishop-Bailey, D.; Swales, K. E., The Role of PPARs in the Endothelium: Implications for Cancer Therapy. *PPAR Res* **2008**, 2008, 904251.
- 97. Ahmed, W.; Orasanu, G.; Nehra, V.; Asatryan, L.; Rader, D. J.; Ziouzenkova, O.; Plutzky, J., High-density lipoprotein hydrolysis by endothelial lipase activates PPARalpha: a candidate mechanism for high-density lipoprotein-mediated repression of leukocyte adhesion. *Circ Res* **2006**, 98, (4), 490-8.
- 98. Delerive, P.; Furman, C.; Teissier, E.; Fruchart, J.; Duriez, P.; Staels, B., Oxidized phospholipids activate PPARalpha in a phospholipase A2-dependent manner. *FEBS Lett* **2000**, 471, (1), 34-8.
- 99. el Azzouzi, H.; Leptidis, S.; Bourajjaj, M.; Armand, A. S.; van der Nagel, R.; van Bilsen, M.; Da Costa Martins, P. A.; De Windt, L. J., Peroxisome proliferator-activated receptor (PPAR) gene profiling uncovers insulin-like growth factor-1 as a PPARalpha target gene in cardioprotection. *J Biol Chem* **2011**, 286, (16), 14598-607.
- 100. Goya, K.; Sumitani, S.; Xu, X.; Kitamura, T.; Yamamoto, H.; Kurebayashi, S.; Saito, H.; Kouhara, H.; Kasayama, S.; Kawase, I., Peroxisome proliferator-activated receptor alpha agonists increase nitric oxide synthase expression in vascular endothelial cells. *Arterioscler Thromb Vasc Biol* **2004**, 24, (4), 658-63.
- 101. Mehrotra, D.; Wu, J.; Papangeli, I.; Chun, H. J., Endothelium as a gatekeeper of fatty acid transport. *Trends Endocrinol Metab* **2014,** 25, (2), 99-106.
- 102. Burns, K. A.; Vanden Heuvel, J. P., Modulation of PPAR activity via phosphorylation. *Biochim Biophys Acta* **2007**, 1771, (8), 952-60.
- 103. Ramirez, S. H.; Fan, S.; Zhang, M.; Papugani, A.; Reichenbach, N.; Dykstra, H.; Mercer, A. J.; Tuma, R. F.; Persidsky, Y., Inhibition of glycogen synthase kinase 3beta

(GSK3beta) decreases inflammatory responses in brain endothelial cells. *Am J Pathol* **2010,** 176, (2), 881-92.

104. Mancia, G.; De Backer, G.; Dominiczak, A.; Cifkova, R.; Fagard, R.; Germano, G.; Grassi, G.; Heagerty, A. M.; Kjeldsen, S. E.; Laurent, S.; Narkiewicz, K.; Ruilope, L.; Rynkiewicz, A.; Schmieder, R. E.; Boudier, H. A.; Zanchetti, A.; Vahanian, A.; Camm, J.; De Caterina, R.; Dean, V.; Dickstein, K.; Filippatos, G.; Funck-Brentano, C.; Hellemans, I.; Kristensen, S. D.; McGregor, K.; Sechtem, U.; Silber, S.; Tendera, M.; Widimsky, P.; Zamorano, J. L.; Erdine, S.; Kiowski, W.; Agabiti-Rosei, E.; Ambrosioni, E.; Lindholm, L. H.; Viigimaa, M.; Adamopoulos, S.; Agabiti-Rosei, E.; Ambrosioni, E.; Bertomeu, V.; Clement, D.; Erdine, S.; Farsang, C.; Gaita, D.; Lip, G.; Mallion, J. M.; Manolis, A. J.; Nilsson, P. M.; O'Brien, E.; Ponikowski, P.; Redon, J.; Ruschitzka, F.; Tamargo, J.; van Zwieten, P.; Waeber, B.; Williams, B., 2007 Guidelines for the Management of Arterial Hypertension: The Task Force for the Management of Arterial Hypertension of the European Society of Hypertension (ESH) and of the European Society of Cardiology (ESC). *J Hypertens* 2007, 25, (6), 1105-87.

105. Versari, D.; Daghini, E.; Virdis, A.; Ghiadoni, L.; Taddei, S., Endothelial dysfunction as a target for prevention of cardiovascular disease. *Diabetes Care* **2009**, 32 Suppl 2, S314-21.

Figure legends

Figure 1. The number of isolated endothelial cells after irradiation. The counts of isolated endothelial cells from mice irradiated with 0 Gy (control), 8 Gy or 16 Gy show that the amount of endothelial cells isolated from mice that were irradiated with 16 Gy was significantly lower than the amount isolated from control or 8 Gy-irradiated mice. The error bars represent standard error of the mean (SEM). Four biological replicates in each group were used for the statistical analysis; ($p^* < 0.05$, t-test; n=4).

Figure 2. Identification and characterisation of endothelial cells isolated from mouse hearts irradiated with 0 Gy (control), 8 Gy or 16 Gy. Proportion of positively stained cells of all cells (%) is shown for endothelial cell markers PECAM-1, endoglin, VE-cadherin, ICAM-1, ICAM-2, mucosialin and VCAM-1. The proportion of cells that stained positively for these markers was nearly 100% (97±2), independent of the radiation dose. The amount of endothelial cells that stained positively for VCAM-1 was significantly increased after 8 Gy (32%) compared with control cells. The error bars represent standard error of the mean (SEM). Three biological replicates in each group were used for the statistical analysis; ($p^* < 0.05$, t-test) (A). Mean fluorescence intensity values are shown for endothelial cell markers PECAM-1, endoglin, VE-cadherin, ICAM-1, ICAM-2, mucosialin and VCAM-1. Cell surface densities of ICAM-1 and ICAM-2 showed significant increases after 16 weeks at 8 Gy and 16 Gy compared to control cells. The error bars represent standard error of the mean (SEM); ($p^* < 0.05$, t-test; n=3) (B).

Figure 3. Protein-protein interaction analysis of the significantly differentially expressed proteins. The biological networks are shown after 8 Gy (A) and 16 Gy (B). Association networks were analysed by the STRING software tool (http://string-db.org). The analysis of all significantly deregulated proteins from both protein profiles indicated five

distinct but interconnected clusters of proteins: cytoskeletal structure, translation and transcription, heat shock proteins, mitochondrial respiratory chains, and metabolism.

Figure 4. Ingenuity pathway analysis of upstream transcriptional regulators. Graphical representation of the deregulated protein networks with their upstream transcriptional regulators after 8 Gy (A) and 16 Gy (B) (http://www.INGENUITY.com). The up-regulated proteins are marked in red and the down-regulated in green. The nodes in blue represent transcription factors. The gene IDs of the proteins are available in supplementary tables S2 and S3.

Figure 5. Immunoblot verification of the relevant proteins of the Insulin-PI3K-Akt pathway after 8 and 16 Gy. Immunoblot analysis of EC protein lysate was performed using anti-INSR / IGF1R , anti-phospho INSR / IGF1R (Tyr1146/1131), anti-PI3K (p85), anti-phospho PI3K [p85 (Tyr458)/p55 (Tyr199)], anti-Akt, anti-phospho AKt (Ser473), anti-mTOR, anti-phospho mTOR (Ser2488), anti-GSK3 beta, anti-phospho GSK3 beta (Ser21/9), anti-FOXO3a, anti-phospho FOXO3a (Ser318/321), anti-eNOS, anti-phospho eNOS (Ser1177) and anti-Glut4 (A). The columns represent the average ratios of relative protein expression in sham- and irradiated samples after background correction and normalisation to GAPDH expression (B and C) (*t*-test; **p*< 0.05; n=3). The analysis showed the significantly reduced activity of insulin/ PI3K cascade (D).

Figure 6. Immunoblot analysis of phosphorylation events of MAPK pathway, oxidative stress response and senescence. Immunoblot analysis of EC protein lysate was performed using anti-ERK 44/42, anti-phospho-ERK (p-ERK), anti-p38, anti-phospho-p38 (p-p38), anti-superoxide dismutase 1 (SOD), anti-heat shock proteins 90 and 70 (Hsp90 and Hsp70) and anti-p16, anti-p21 and anti-p53, and anti-phospho-p53 (A, B).Columns represent the average ratios of relative protein expression in sham- and irradiated samples after

background correction and normalisation to GAPDH expression (C, D, E and F) (*t*-test; **p*< 0.05; n=3). The analysis showed significantly increased level of phosphorylated p38 after 16 Gy (D) indicating effect of ionising radiation on insulin/IGF-MAPK signalling pathway (G). The protein levels of SOD and Hsp90 were significantly decreased while hsp70 was increased after radiation. The protein markers of senescence (p16 and p21) were markedly increased after both doses.

Figure 7. Analysis of insulin receptor substrate 1 (IRS-1) phosphorylation. The phosphorylation status of insulin receptors was analysed using total IRS (A), phospho-IRS-1 (serine-621) (B), phospho-IRS-1 (serine-307) (C) and phospho-IRS-1 (pan-tyrosine) (D) Sandwich ELISA Kits . AU: arbitrary unit (A-D) (*t*-test; **p*<0.05; n=3). The level of total IRS-1 and phospho-IRS1 (Ser621) did not change after irradiation (B). Phosphorylation of IRS-1 at Ser-307 was increased while phosphorylation of IRS-1 at tyrosine residues was reduced (D).

Figure 8. Analysis of the levels of stress-induced protein modifications. The total amount of the 3-nitrotyrosine-modified proteins (protein nitrosylation marker) (A), malondialdehyde modified proteins (lipid peroxidation marker) (B), homocysteinylated proteins (C) and carbonylated proteins (D) were analysed after irradiation. Analysis showed markedly increase level of malondialdehyde-modified proteins, nitrosylated proteins and homocysteinylated proteins and carbonylated proteins after radiation suggesting protein damage by oxidative stress. (t-test; *p<0.05; n=3).

Figure 9. **Serum glucose**, **nitric oxide**, **oxLDL and cytokines assay**. The serum levels of glucose (A), nitric oxide (NO) (B), oxLDL (C) and cytokines (D) were analysed using ELISA assay after irradiation. The analysis showed increased level of glucose after 16 Gy (A). The serum NO level was significantly reduced after both doses (B). The analysis showed elevated level of oxLDL after both doses (C). The levels of TNF alpha, IL1a and IL6 were enhanced after irradiation (D). (t-test; *p< 0.05; n = 4).

Figure 10. Proposed model for the role of insulin/IGF-PI3K-Akt cascade in radiation-induced endothelial dysfunction. All proteins and genes found significantly deregulated in this study are indicated with stars in pathway.

Table 1. Overlapping significantly deregulated proteins between the two radiation doses. The number of shared endothelial proteins with their accession numbers, gene IDs and names with corresponding fold changes (H/L) after doses of 8 and 16 Gy are indicated.

No.	Gene ID	Description	H/L 8 Gy	H/L 16 Gy
1	ACADM	acyl-Coenzyme A dehydrogenase, medium chain	0.7	0.7
2	ATP5O	ATP synthase, H+ transporting, complex, O subunit	0.7	0.7
3	Bin2	bridging integrator 2	1.6	1.9
4	CLTC	clathrin, heavy polypeptide (Hc)	8.3	3.0
5	DES	desmin	0.8	0.5
6	DPYSL2	dihydropyrimidinase-like 2	1.3	2.0
7	EEF1A1	eukaryotic translation elongation factor 1 alpha 1	1.6	1.4
8	EHD2	EH-domain containing 2	1.5	2.1
9	H2D1	H2-D1 MGI Symbol histocompatibility 2, D region locus 1	1.3	1.9
10	HADHB	hydroxyacyl-Coenzyme A dehydrogenase beta subunit	0.7	0.6
11	HIST1H1C	histone cluster 1, H1c	0.6	0.7
12	HIST1HE	histone cluster 1, H1e	0.6	0.6
13	HSP90AA1	heat shock protein 90, alpha (cytosolic), class A member 1	0.6	0.6
14	HSP90B1	heat shock protein 90, beta (Grp94), member 1	0.6	0.7
15	HSPA12B	heat shock protein 70, 12B	2.3	1.3
16	HSPA5	heat shock protein 5	0.7	0.7
17	LMNB2	lamin B2	0.6	0.7
18	MYH9	myosin, heavy polypeptide 9, non-muscle	4.1	1.4
19	PDHA1	pyruvate dehydrogenase E1 alpha 1	0.8	0.6
20	RPL3	ribosomal protein L3	0.7	0.8
21	THBS1	thrombospondin 1	2.6	2.2
22	TKT	transketolase	1.8	2.2
23	TUBB4B	tubulin, beta 4B class IVB	2.2	1.3
24	Uqcrc2	ubiquinol cytochrome c reductase core protein 2	0.5	0.7
25	VASP	vasodilator-stimulated phosphoprotein	1.3	1.5
26	Vim	vimentin	1.3	1.3

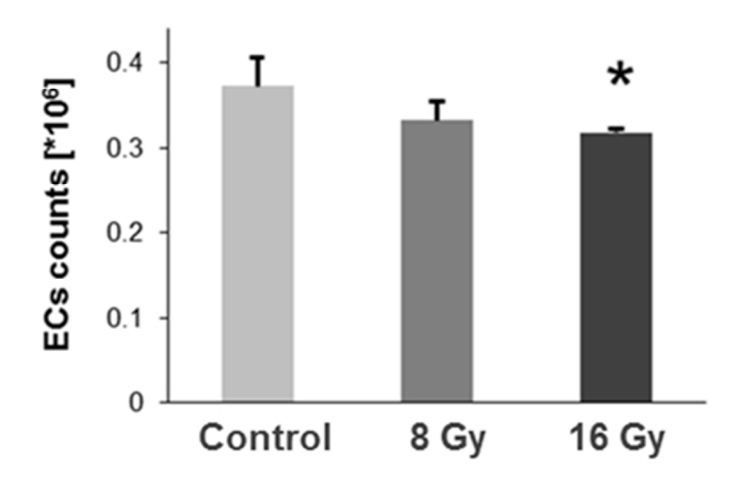
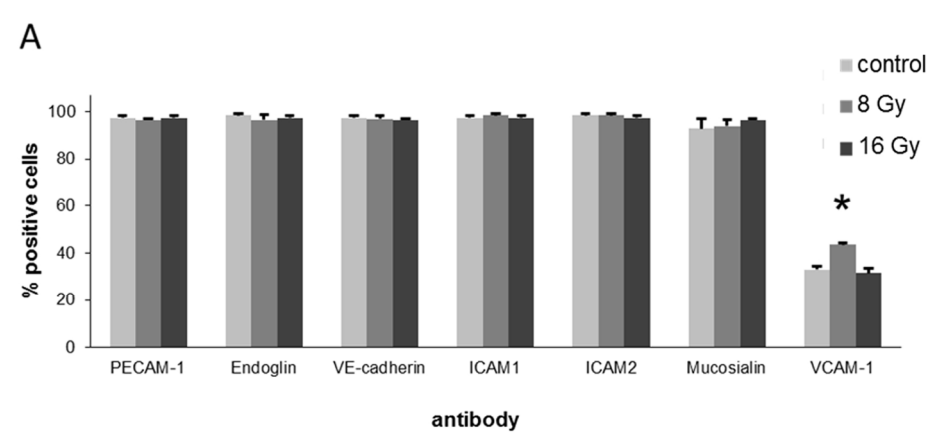


Figure 1
The number of isolated endothelial cells after irradiation. The counts of isolated endothelial cells from mice irradiated with 0 Gy (control), 8 Gy or 16 Gy show that the amount of endothelial cells isolated from mice that were irradiated with 16 Gy was significantly lower than the amount isolated from control or 8 Gy-irradiated mice. The error bars represent standard error of the mean (SEM). Four biological replicates in each group were used for the statistical analysis; (p* < 0.05, t-test; n=4). 50x33mm (300 x 300 DPI)



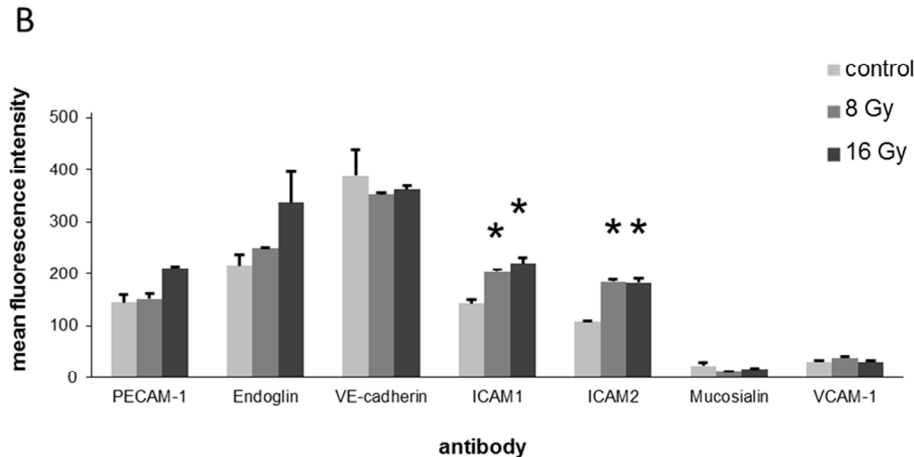


Figure 2

Identification and characterisation of endothelial cells isolated from mouse hearts irradiated with 0 Gy (control), 8 Gy or 16 Gy. Proportion of positively stained cells of all cells (%) is shown for endothelial cell markers PECAM-1, endoglin, VE-cadherin, ICAM-1, ICAM-2, mucosialin and VCAM-1. The proportion of cells that stained positively for these markers was nearly 100% (97±2), independent of the radiation dose. The amount of endothelial cells that stained positively for VCAM-1 was significantly increased after 8 Gy (32%) compared with control cells. The error bars represent standard error of the mean (SEM). Three biological replicates in each group were used for the statistical analysis; (p* < 0.05, t-test) (A). Mean fluorescence intensity values are shown for endothelial cell markers PECAM-1, endoglin, VE-cadherin, ICAM-1, ICAM-2, mucosialin and VCAM-1. Cell surface densities of ICAM-1 and ICAM-2 showed significant increases after 16 weeks at 8 Gy and 16 Gy compared to control cells. The error bars represent standard error of the mean (SEM); (p* < 0.05, t-test; n=3) (B).

177x162mm (300 x 300 DPI)

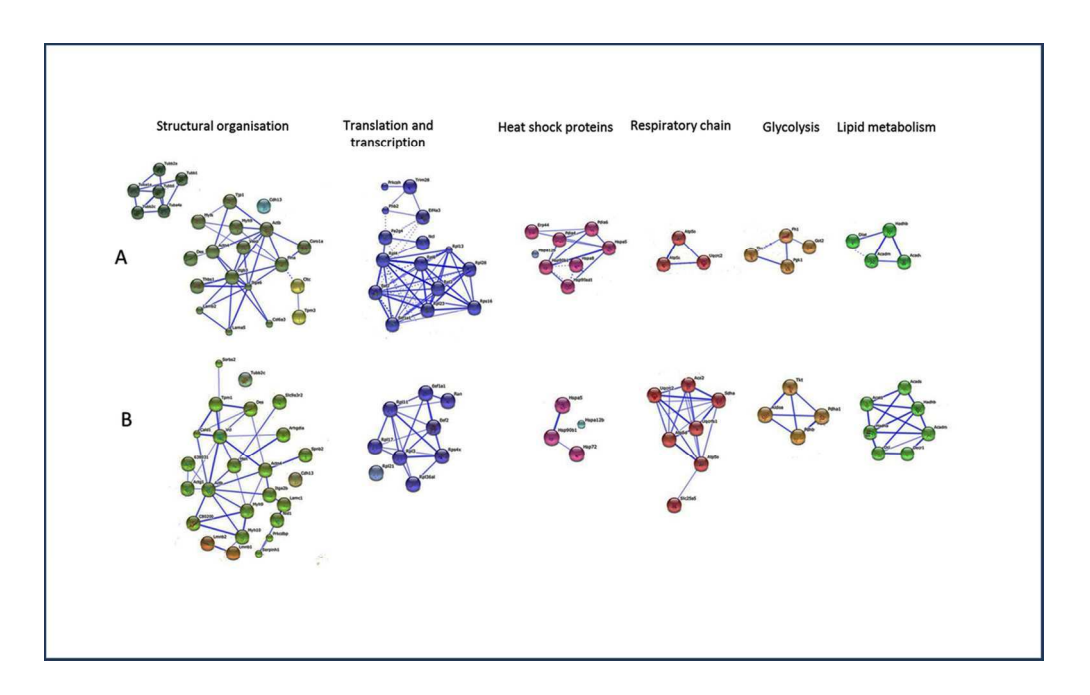


Figure 3
Protein-protein interaction analysis of the significantly differentially expressed proteins. The biological networks are shown after 8 Gy (A) and 16 Gy (B). Association networks were analysed by the STRING software tool (http://string-db.org). The analysis of all significantly deregulated proteins from both protein profiles indicated five distinct but interconnected clusters of proteins: cytoskeletal structure, translation and transcription, heat shock proteins, mitochondrial respiratory chains, and metabolism.

108x67mm (300 x 300 DPI)

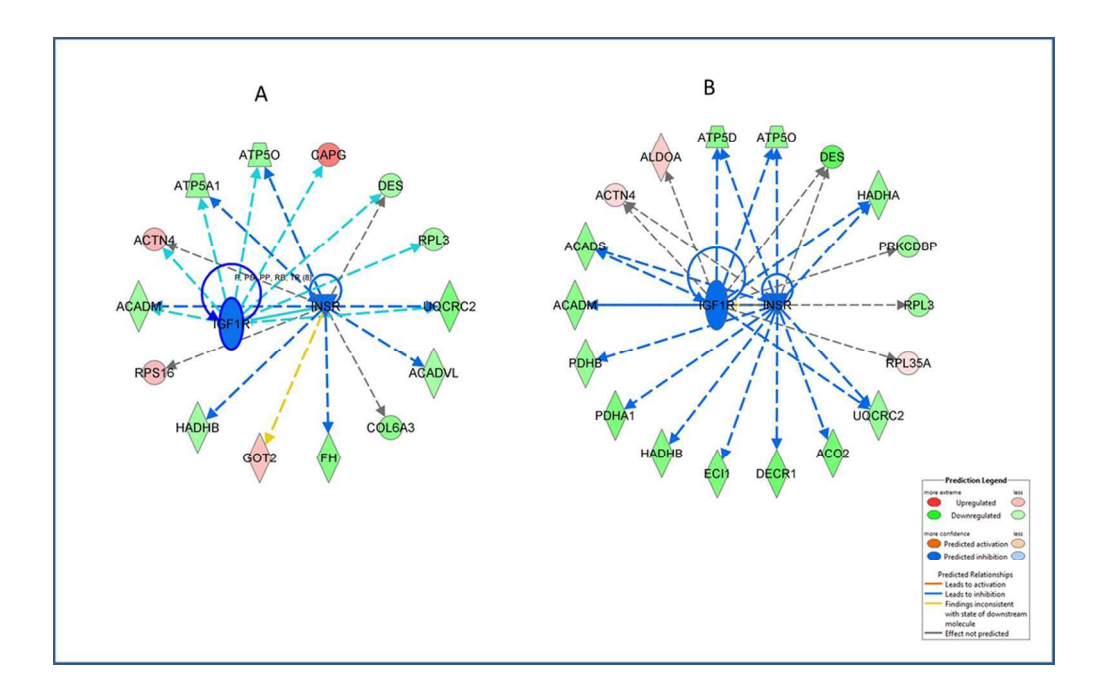


Figure 4
Ingenuity pathway analysis of upstream transcriptional regulators. Graphical representation of the deregulated protein networks with their upstream transcriptional regulators after 8 Gy (A) and 16 Gy (B) (http://www.INGENUITY.com). The up-regulated proteins are marked in red and the down-regulated in green. The nodes in blue represent transcription factors. The gene IDs of the proteins are available in supplementary tables S2 and S3.

177x110mm (300 x 300 DPI)

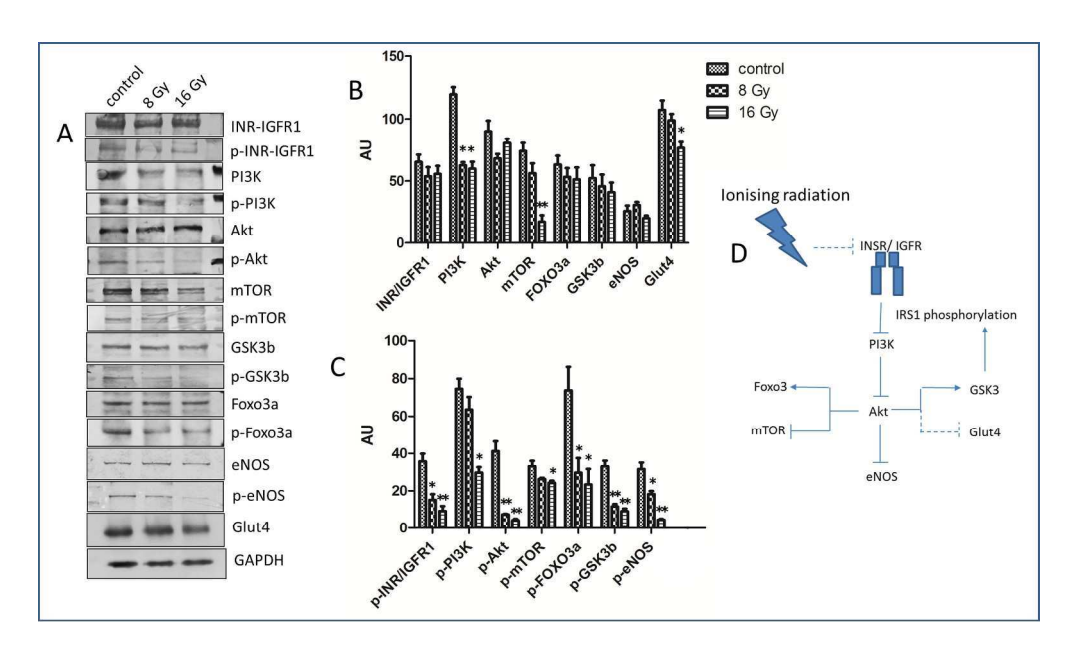


Figure 5

Immunoblot verification of the relevant proteins of the Insulin-PI3K-Akt pathway after 8 and 16 Gy. Immunoblot analysis of EC protein lysate was performed using anti-INSR / IGF1R , anti-phospho INSR / IGF1R (Tyr1146/1131), anti-PI3K (p85), anti-phospho PI3K [p85 (Tyr458)/p55 (Tyr199)], anti-Akt, anti-phospho AKt (Ser473), anti-mTOR, anti-phospho mTOR (Ser2488), anti-GSK3 beta, anti-phospho GSK3 beta (Ser21/9), anti-FOXO3a, anti-phospho FOXO3a (Ser318/321), anti-eNOS, anti-phospho eNOS (Ser1177) and anti-Glut4 (A). The columns represent the average ratios of relative protein expression in sham- and irradiated samples after background correction and normalisation to GAPDH expression (B and C) (t-test; *p< 0.05; n=3). The analysis showed the significantly reduced activity of insulin/ PI3K cascade (D). 380x220mm (300 x 300 DPI)

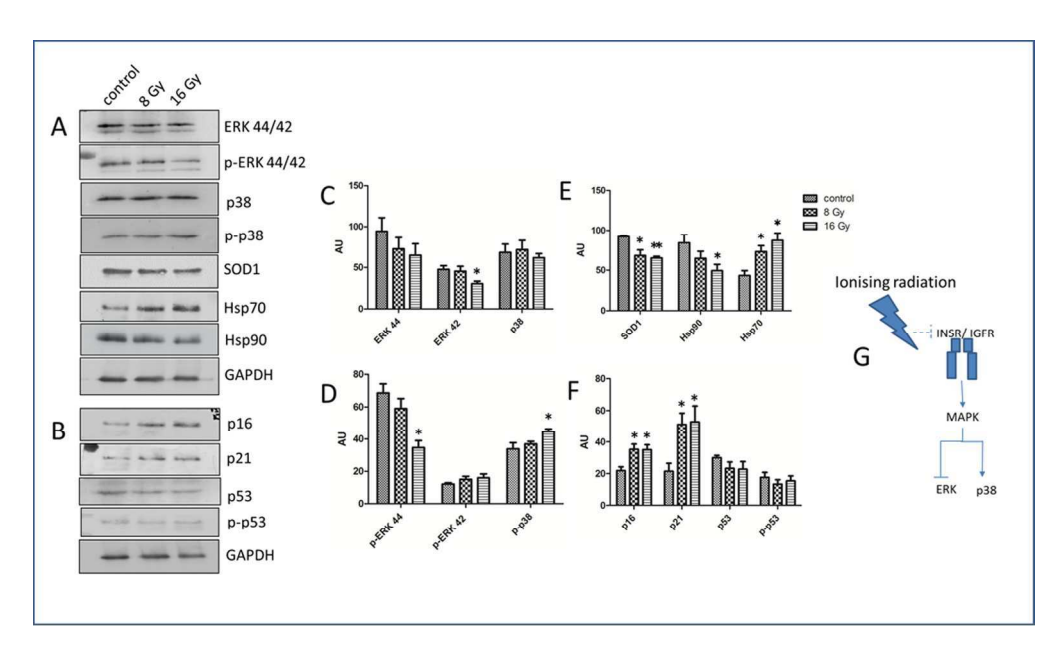


Figure 6

Immunoblot analysis of phosphorylation events of MAPK pathway, oxidative stress response and senescence. Immunoblot analysis of EC protein lysate was performed using anti-ERK 44/42, anti-phospho-ERK (p-ERK), anti-p38, anti-phospho-p38 (p-p38), anti-superoxide dismutase 1 (SOD), anti-heat shock proteins 90 and 70 (Hsp90 and Hsp70) and anti-p16, anti-p21 and anti-p53, and anti-phospho-p53 (A, B).Columns represent the average ratios of relative protein expression in sham- and irradiated samples after background correction and normalisation to GAPDH expression (C, D, E and F) (t-test; *p< 0.05; n=3). The analysis showed significantly increased level of phosphorylated p38 after 16 Gy (D) indicating effect of ionising radiation on insulin/IGF-MAPK signalling pathway (G). The protein levels of SOD and Hsp90 were significantly decreased while hsp70 was increased after radiation. The protein markers of senescence (p16 and p21) were markedly increased after both doses.

177x103mm (300 x 300 DPI)

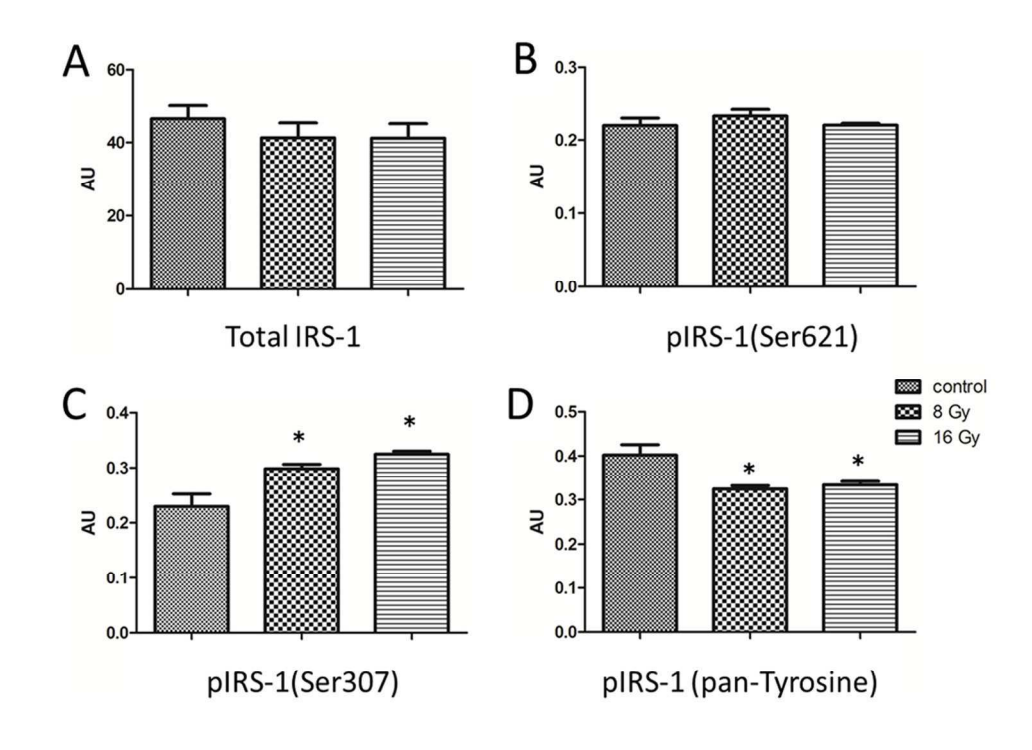


Figure 7
Analysis of insulin receptor substrate 1 (IRS-1) phosphorylation. The phosphorylation status of insulin receptors was analysed using total IRS (A), phospho-IRS-1 (serine-621) (B), phospho-IRS-1 (serine-307) (C) and phospho-IRS-1 (pan-tyrosine) (D) Sandwich ELISA Kits . AU: arbitrary unit (A-D) (t-test; *p<0.05; n=3). The level of total IRS-1 and phospho-IRS1 (Ser621) did not change after irradiation (B). Phosphorylation of IRS-1 at Ser-307 was increased while phosphorylation of IRS-1 at tyrosine residues was reduced (D).

177x138mm (300 x 300 DPI)

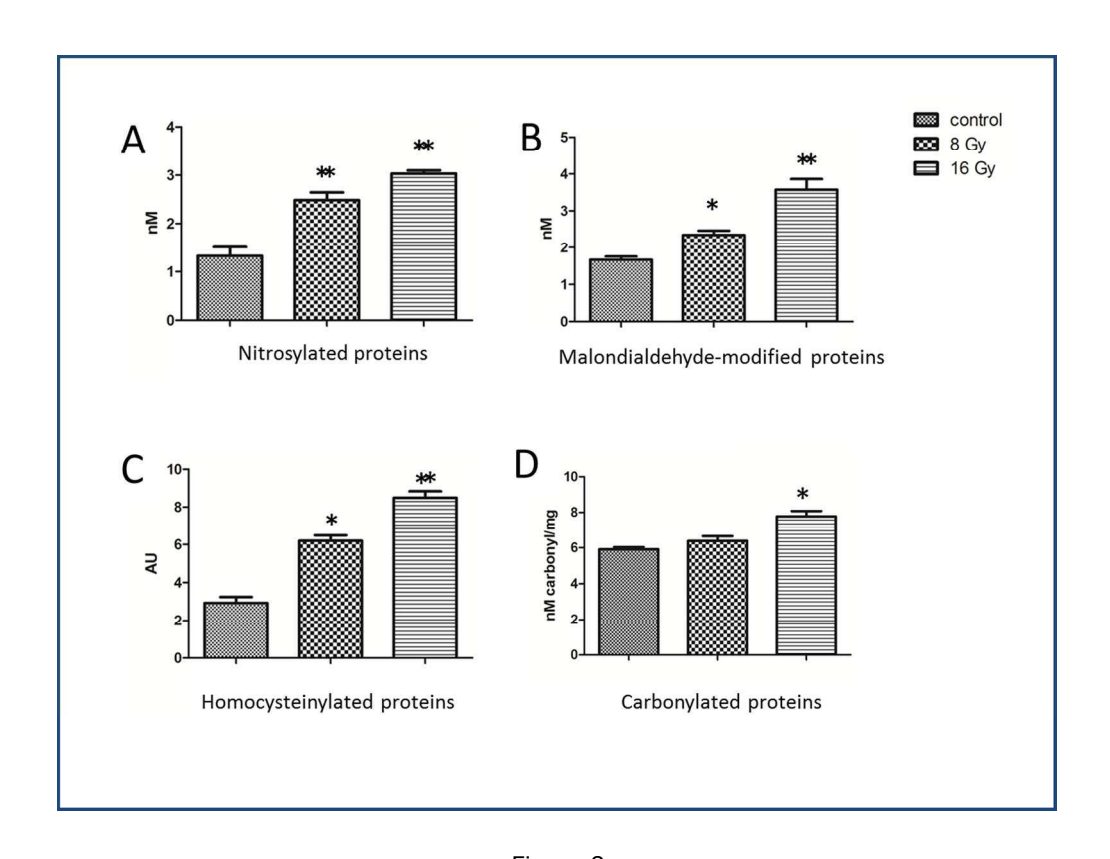


Figure 8
Figure 8. Analysis of the levels of stress-induced protein modifications. The total amount of the 3-nitrotyrosine-modified proteins (protein nitrosylation marker) (A), malondialdehyde modified proteins (lipid peroxidation marker) (B), and homocysteinylated proteins (C) and carbonylated proteins (D) were analysed after irradiation. Analysis showed markedly increase level of malondialdehyde-modified proteins, nitrosylated proteins and homocysteinylated proteins and carbonylated proteins after radiation suggesting protein damage by oxidative stress. (t-test; *p<0.05; n=3).

220x166mm (300 x 300 DPI)

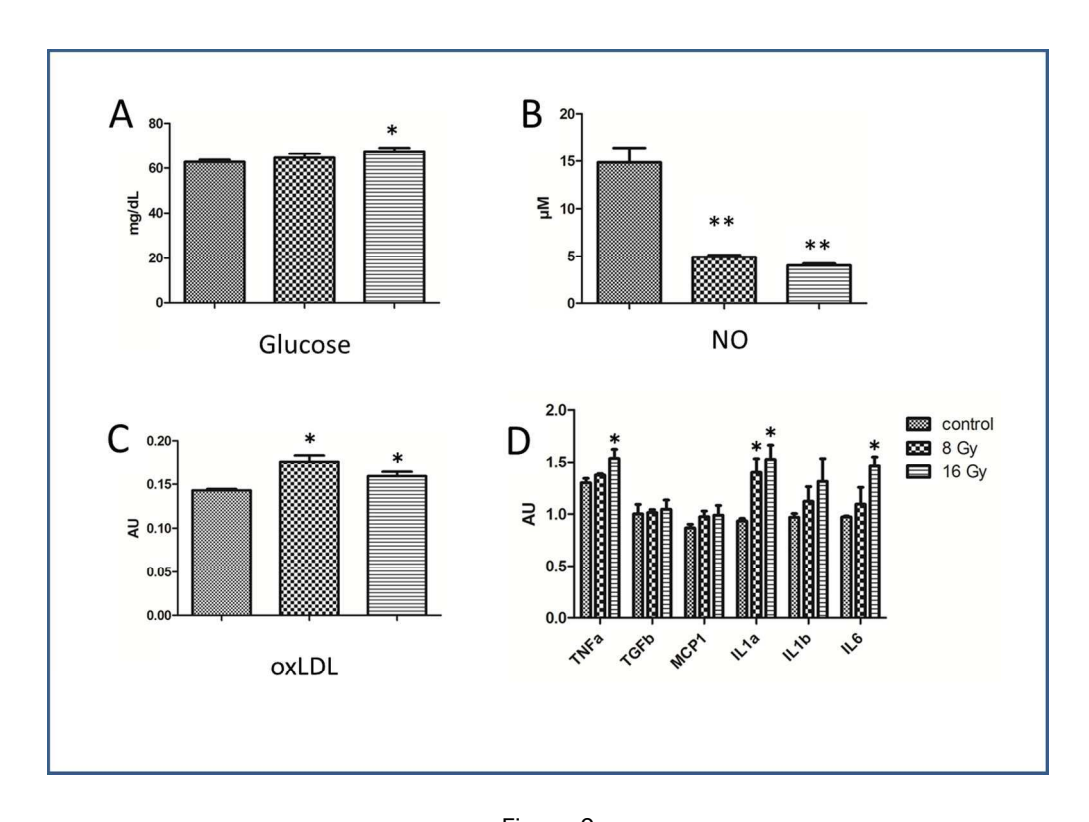


Figure 9

Serum glucose, nitric oxide, oxLDL and cytokines assay. The serum levels of glucose (A), nitric oxide (NO) (B), oxLDL (C) and cytokines (D) were analysed using ELISA assay after irradiation. The analysis showed increased level of glucose after 16 Gy (A). The serum NO level was significantly reduced after both doses (B). The analysis showed elevated level of oxLDL after both doses (C). The levels of TNF alpha, IL1a and IL6 were enhanced after irradiation (D). (t-test; *p< 0.05; n = 4).

224x162mm (300 x 300 DPI)

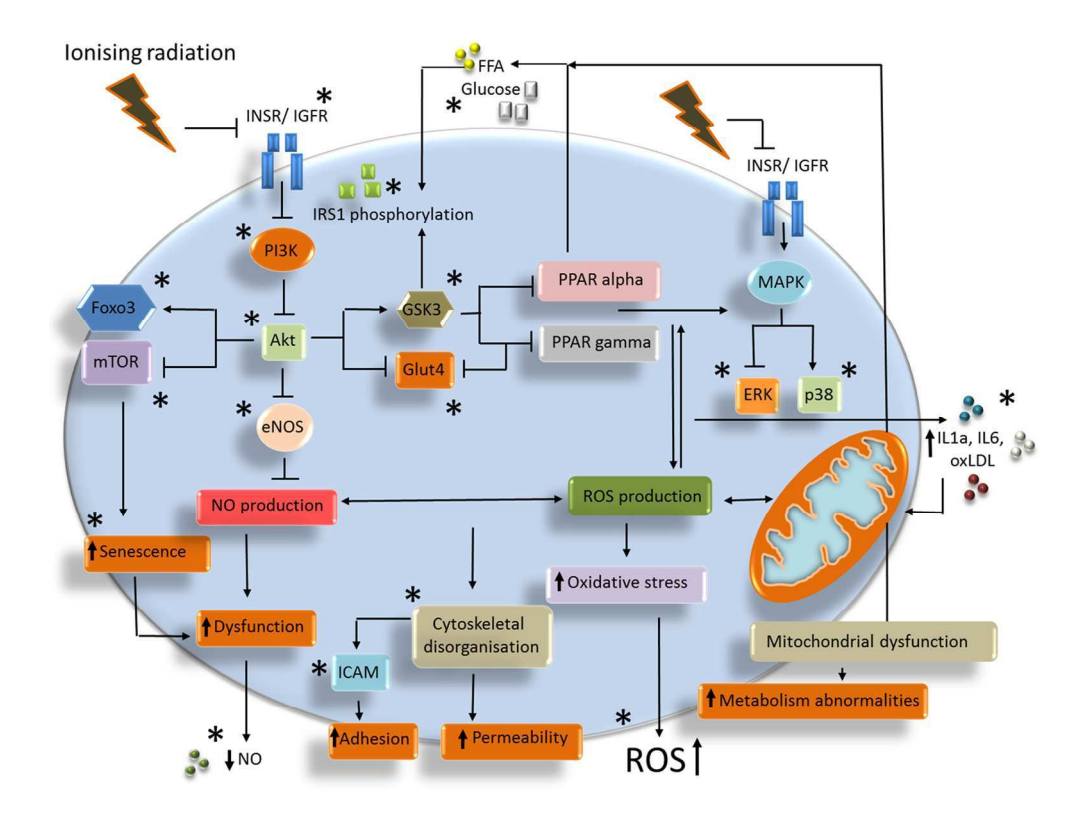
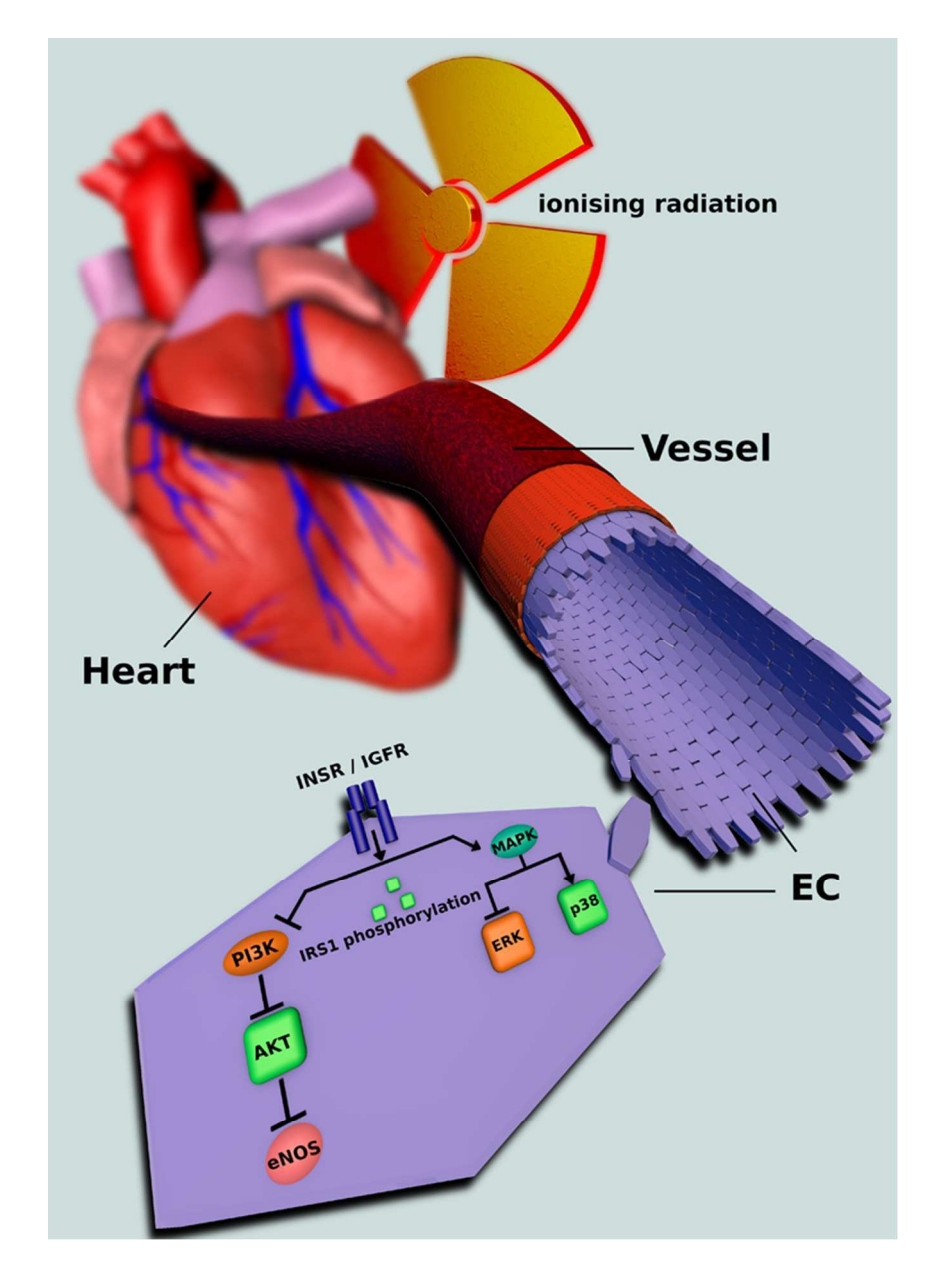


Figure 10 Proposed model for the role of insulin/IGF-PI3K-Akt cascade in radiation-induced endothelial dysfunction. All proteins and genes found significantly deregulated in this study are indicated with stars in pathway. $238 \times 184 \text{mm} (300 \times 300 \text{ DPI})$



Graphical Abstract 63x90mm (300 x 300 DPI)